1521-0111/96/3/330–344$35.00
MOLECULAR PHARMACOLOGY

https://doi.org/10.1124/mol.119.116400
Mol Pharmacol 96:330–344, September 2019

Temperature Dependence of the Biophysical Mechanisms Underlying the Inhibition and Enhancement Effect of Amiodarone on hERG Channels [S]

Yung-Chen Lo and Chung-Chin Kuo

Department of Physiology, National Taiwan University College of Medicine, Taipei, Taiwan; and Department of Neurology, National Taiwan University Hospital, Taipei, Taiwan

Received February 27, 2019; accepted June 21, 2019

ABSTRACT

hERG K^+ channel is important for controlling the duration of cardiac action potentials. Amiodarone (AMD), a widely prescribed class III antiarrhythmic, could inhibit hERG currents with relatively few tachyarrhythmic adverse events. We use injected *Xenopus* oocyte with two-electrode voltage clamp techniques to characterize the action of AMD on hERG channels. We found that AMD binds to the resting hERG channel with an apparent dissociation constant of ~1.4 μM, and inhibits hERG currents at mild and strong depolarization pulses by slowing activation and enhancing inactivation, respectively, at 22°C. The activation kinetics of hERG channel activation are much faster, but inactivation kinetics are slower at 37°C. AMD accordingly has a 15% to 20% weaker and stronger inhibitory effect at mild and strong depolarization (e.g., −60 and +30 mV, 0.3-second pulse), respectively. In the meanwhile, the resurgent hERG tail currents are dose-dependently inhibited by AMD without altering the kinetics of current decay at both 22°C and 37°C, indicating facilitation of recovery from inactivation via the silent route. Most importantly, AMD no longer inhibits but enhances hERG currents at a mild pulse shortly after a prepulse at 37°C, but not so much at 22°C. We conclude that AMD is an effective hERG channel–gating modifier capable of lengthening the plateau phase of cardiac action potential (without increasing the chance of afterdepolarization). AMD, however, should be used with caution in hypothermia or the other scenarios that slow hERG channel activation.

SIGNIFICANCE STATEMENT

It is known that amiodarone (AMD) acts on hERG K^+ channels to treat cardiac arrhythmias with relatively little arrhythmogenicity. We found that AMD enhances hERG channel inactivation but slows activation as well as recovery from inactivation, and thus has a differential inhibition and enhancement effect on hERG currents at different phases of membrane voltage changes, especially at 37°C, but not so much at 22°C. AMD is therefore a relatively ideal agent against tachyarrhythmia at 37°C, but should be more cautiously used at lower temperatures or relevant pathophysiological/pharmacological scenarios associated with slower hERG channel activation because of the increased chances of adverse events.

Introduction

Gating of the hERG K^+ channel is well known for the acceleration of inactivation over activation during a pulse of strong depolarization (Wang et al., 1997). hERG currents, although based on a depolarization-activated channel, are thus paradoxically decreased at stronger depolarization because more channels are rapidly driven into the inactivation state (Trudeau et al., 1995; Schönherr and Heinemann, 1996; Smith et al., 1996). hERG K^+ channel gating is also characterized by a large resurgent tail current upon repolarization, presumably signaling recovery from inactivation trespassing an open state. hERG currents would therefore be more inhibited in the presence of more repetitive or prolonged depolarization. Upon repolarization, resurgent hERG currents presumably are generated to stabilize the resting phase. These characters make hERG channels an important control of appropriate repetitive discharges in heart and many different types of neurons (Babcock and Li, 2013). From the molecular perspective, the basis of the intriguing gating phenomena has been focused on the possibilities of slow activation with relative fast C-type inactivation, such as relocalization of voltage sensor domains or reconfiguration of S-5-P loop on the outer mouth region (Schönherr and Heinemann, 1996; Wang et al., 1997; Torres et al., 2003; Zhang et al., 2004; Jiang et al., 2005), but many of the essential biophysical attributes of gating have remained uncharacterized. For example, hERG channel could recover from inactivation via two routes in theory. Deinactivation before deactivation would necessarily involve trespass of an open state and genesis of currents, and thus the resurgent route. Deactivation before deinactivation, in contrast, would indicate that no open state is trespassed and thus the silent route of recovery, which has been much less characterized (Clancy and Rudy, 2001). Whether there is only

This work was supported by grants from the Ministry of Science and Technology, Taiwan (MOST) MOST107–2321–B–002–012 (to C.-C.K.) and MOST106–2320–B–002–014–MY3 (to C.-C.K.), and the National Health Research Institute of Taiwan NHRI–EX107–10503NI (to C.-C.K.).
https://doi.org/10.1124/mol.119.116400.
[S] This article has supplemental material available at molpharm.aspetjournals.org.

ABBREVIATIONS: AMD, amiodarone; APD_{90}, action potential duration at 90%; TdP, torsade de pointes.

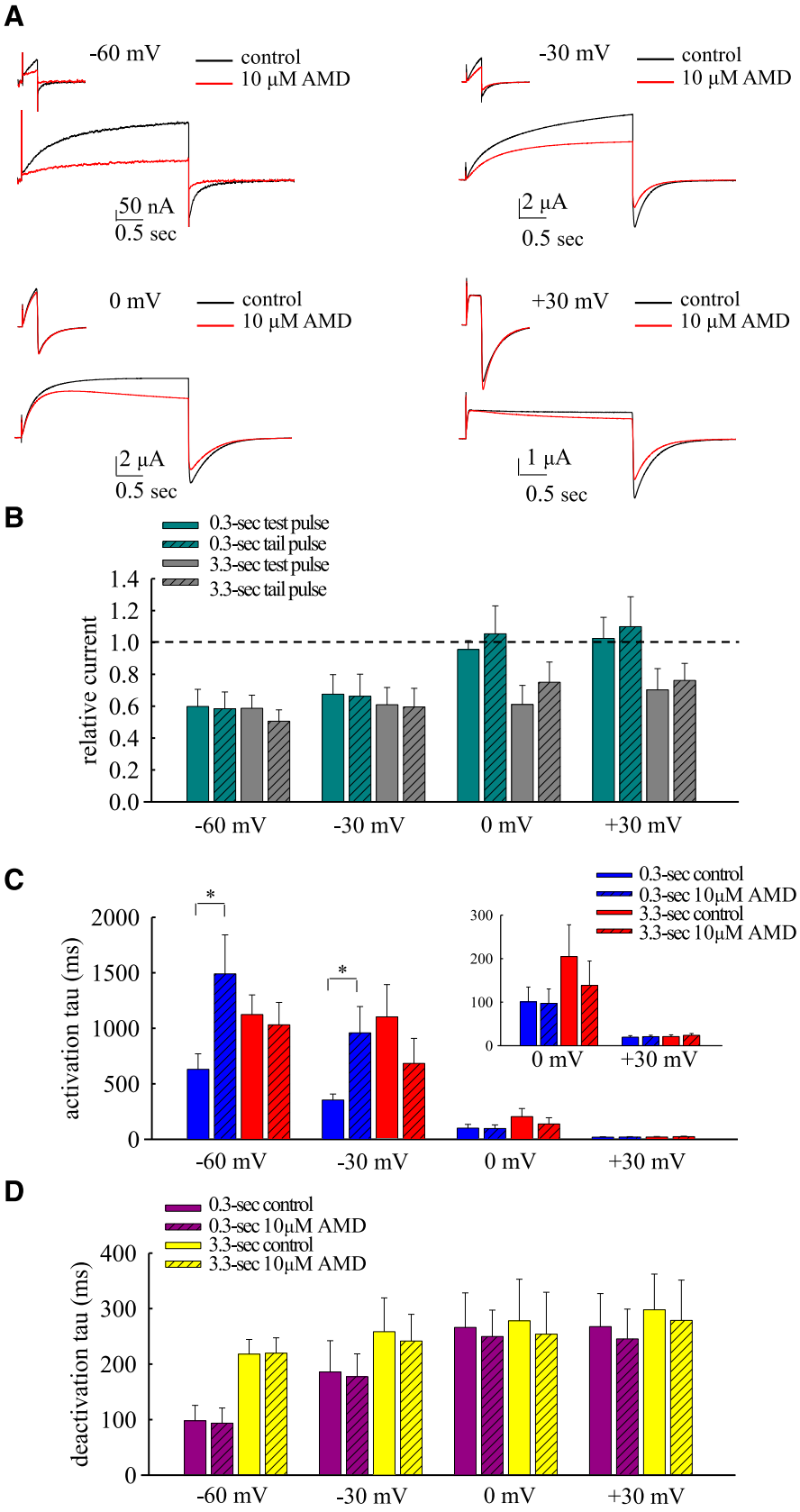

Fig. 1. The voltage-dependent inhibitory effect of AMD on short and long depolarization pulses at 22°C. (A) hERG currents were elicited by short (0.3-second) and long (3.3-second) test pulses at −60, −30, 0, +30 mV from a holding potential at −90 mV. (B) The late sustained currents (the average currents in the last 5 ms of the test pulse) and the peak of tail currents in 10 μM AMD are normalized to that in control to give the relative currents in the test and tail pulses (0.3 second, green bar; 3.3 seconds, gray bar; n = 10, 10, 11, 10 for −60, −30, −0, +30 mV, respectively). (C) The time constants from the monoexponential fits to the growing phase of the currents (5% to 95% of currents) in (A) show that 10 μM AMD slows channel activation from holding potential of (−90 mV) at mild pulses (e.g., −60 mV) but not strong pulses (e.g., +30 mV) (paired two-tailed t test, $^*P < 0.05$). Note this is just an approximate estimate of channel activation kinetics because of the possible contamination by inactivation especially with a longer (3.3-second) pulse. Inset figure: a magnified view of the data at 0 and +30 mV. (D) The time constants from the monoexponential fits to the decay phase of the tail currents (from 5% to 95% of the currents) in (A) show that although 10 μM AMD has no apparent effect on the deactivation kinetics of hERG currents, more depolarized and prolonged preceding pulses by themselves tend to lead to slower decay (longer time constant or τ of the decay phase) of the tail currents. The results of different pulse durations are shown in purple (0.3 second) and yellow (3.3 seconds), respectively (n = 10, 10, 11, 10 for −60, −30, −0, +30 mV, respectively). Data of the same test pulse voltages were acquired from the same cells.

one open state to be trespassed, and whether and how the different routes of recovery from inactivation are proportioned to determine the size of the resurgent tail currents, are not clear.

Amiodarone (AMD) is the most frequently prescribed type III antiarrhythmic agent (Heger et al., 1981; Zimetbaum, 2007). With prolongation of action potential duration at 90%,

AMD may prevent re-entrant excitation and thus tachyarrhythmias. The mechanism of action of AMD has been ascribed to inhibition of hERG channel and consequent prolongation of the refractory period, which is a hallmark of the class III antiarrhythmics (Sanguinetti et al., 1995). Interestingly, AMD seems to have a much better safety profile in terms of the risk of induction of severe tachyarrhythmias such as Torsade de Pointes (Roden, 2004). It was proposed that the protonated form of AMD may act as a pore blocker and inhibit hERG channels (Kiehn et al., 1999; Mitcheson et al., 2000; Ridley et al., 2004), and the critical residues involved in AMD inhibition are located at the proximal regions of selectivity filter (Zhang et al., 2016). In contrast, the inactivation-removing mutations such as N588K and N588K/S631A dramatically reduce the inhibitory effect of AMD (McPate et al., 2008), suggesting that C-type inactivation or gating modification does play an important role in the action of AMD. It is also of note that AMD could enhance rather than inhibit hERG currents at mild depolarization in a prepulse-dependent manner (Furutani et al., 2011). This is incompatible with the idea that AMD acts simply as a pore blocker of hERG channels, but strongly implicates gating modification of hERG channels by AMD. Although a smaller K_d between AMD and hERG channel at 37°C than 23°C (Kauthale et al., 2015), the action of AMD on the unique gating profiles of hERG channels has not been systemically and fully characterized, especially at 37°C. We found that AMD binds to the deactivated (closed) state to enhance the voltage dependence of hERG channel gating, and thus inhibits hERG currents at mild depolarization pulses (−30 to −60 mV) but enhances the initial rising phase and then inhibits the late currents due to accelerated inactivation at 0 to +30 mV at 22°C. Because of acceleration of activation but slowing of inactivation, the inhibitory effect of AMD at mild and strong depolarization decreases and increases, respectively at 37°C. Most interestingly, AMD also promotes recovery from inactivation via the silent route to inhibit the resurgent tail currents. The enhancement effect of hERG currents at a premature pulse shortly after a prepulse is also especially prominent at 37°C. AMD therefore may effectively lengthen the plateau phase of cardiac action potential without increasing the chances of afterdepolarization at 37°C.

Materials and Methods

Molecular Biology and Expression of hERG K^+ Channels. The hERG1-pSP64 cDNA clone was amplified and subsequently extracted from cells by the QIAprep R Spin Miniprep Kit (QIAGEN). The inactivation-removed S620T mutant channel was made with the QuikChange mutagenesis kit (Stratagene, La Jolla, CA) in the wild-type hERG1-pSP64 cDNA plasmid. The point mutation was verified by DNA sequencing. These cDNA plasmids were then cut into linear forms by restriction enzyme (EcoRI) and purified by Gel/polymerase chain reaction DNA (Fragments Extraction Kit, Geneaid). The cDNA templates were used to synthesize cRNA transcripts using mMessage mMachine transcription kit SP6 (Ambion). The hERG cRNA (0.1–1 ng/nl) was then injected into *Xenopus* oocytes (stages V–VI), which has been previously defolliculated and maintained in the culture medium (96 NaCl mM, 2 KCl mM, 1 $CaCl_{2\ mM}$, 1 $MgCl_{2\ mM}$, 5 HEPES mM, and 50 μg/ml gentamycin, pH 7.6) at 14°C to 18°C. The injected *Xenopus* oocytes were incubated in culture medium 1 to 3 days prior to electrophysiological studies. We have purchased our *Xenopus* from South Africa, the African Xenopus Facility C.C (+27-443884757; KNYSNA, Western Cape, South Africa).

Electrophysiological Recordings. For recording of macroscopic K^+ currents, the oocyte was placed in a chamber continuously perfused with modified ND-96 solution with 4 mM K^+ (96 NaCl mM, 4 KCl mM, 1 $CaCl_{2\ mM}$, 1 $MgCl_{2\ mM}$, and 5 HEPES mM, pH 7.4). The hERG currents were then recorded with two-microelectrode voltage–clamp method. The voltage-sensing and current-passing electrodes were filled with 3 M KCl and had a consecutive resistance of 0.1 to 1 MΩ. The membrane potential was controlled by the amplifier (OC-725C; Warner Instrument, Hamden, CT). Data were acquired at room temperature (~22°C) or 37°C using the Digidata-1322A analog/digital interface with pCLAMP software (Axon Instrument, Foster City, CA). The temperature control was achieved by automatic temperature controller (TC-324C; Warner Instrument). The sampling rates were 0.1 to 2 kHz. AMD (Sigma-Aldrich, St. Louis, MO) was dissolved in DMSO to make a 5 mM stock solution and then diluted into the modified ND-96 solution to make final concentration of 0.01 to 100 μM. The most commonly used 10 μM AMD solution contained 0.2% DMSO, which does not have a significant effect on the hERG currents examined by a step depolarization of 0 mV × 30 seconds from holding potential of −120 mV (Supplemental Fig. 1). The highest concentration of AMD in this manuscript is 100 μM. The 2% DMSO has an enhancement effect on the initial and inhibition effect on the late currents (~10% and 5%, respectively, which should not affect a valid interpretation of the experimental results). The oocyte was always continuously perfused for 10 to 30 minutes before experiments to achieve steady-state distribution of the drug.

Data Analysis. The concentration–response curve is fitted with Hill equation:

$$\mathrm{I} - \mathrm{Imin}/\mathrm{Imax} - \mathrm{Imin} = 1\Big/[1 + [\mathrm{AMD}]/\mathrm{Kd}]^{\mathrm{nH}}$$

where I is the hERG current in presence of AMD; Imin and Imax are the minimal and maximal hERG current, respectively; [amio] is the concentration of AMD; K_d denotes the apparent affinity of AMD binding to hERG channels; and nH is the Hill coefficient, which was fixed to 1. For the monoexponential fitting to the courses that rise to the maximum or decay to the steady-state, the fit functions are of the forms:

$$I = \mathrm{A}\ \exp(-\mathrm{t}/\tau) + \mathrm{C}(\text{for the decay phase})$$

$$I = \mathrm{A}[1 - \exp(-\mathrm{t}/\tau)] + \mathrm{C}(\text{for the rising phase})$$

where τ is the time constant, A denotes the relative amplitude of the corresponding components, and C is the steady-state level. For statistical comparison of experimental groups, the Student's t test (paired or nonpaired as designated in the figure legend) is used, and $P < 0.05$ is considered to be significant and all statistics are given as mean ± S.D. All statistical tests had been specified before the experimental results were actually obtained, and all statistical results are reported irrespective of outcome. Basically, all experiments have an independent measurement number $n \geq 4$. All experimental results were verified by at least one complete set of paired data obtained from the same cell. The kinetic model of hERG channel gating is constructed by MATLAB R2015 suite (The Math Works), with Euler method for numeric integration with the time step set at 0.01 to 1 ms. Q-matrix method was employed, and the reversal potential was set to −84 mV.

Results

AMD Inhibits hERG Currents by Slowing of Activation at Mild Pulses and Enhancement of Inactivation at Strong Pulses at 22°C. We first explored the effect of AMD at mild to strong, and short to long depolarization pulses (Fig. 1), endeavoring to elucidate the basic gating parameters based on the most simplistic Scheme 1, where C, O, and I stand for the closed, open, and inactivated states, respectively.

$$\mathrm{C} \rightleftharpoons \mathrm{O} \rightleftharpoons \mathrm{I}$$

Scheme 1

The inhibition of hERG currents by 10 μM AMD during a short (~300 ms) test pulse is manifest at a voltage of −60 or −30 mV at 22°C, with apparent slowing of the initial activation phase. In contrast, the activation phase is not apparently slowed at strong pulses (e.g., 0 mV and especially +30 mV; Fig. 1, A–C). The tail currents are presumably close to true tails returning from the open to the closed states with a short and weak preceding pulse (e.g., −60 mV × 0.3 second). A close examination of the kinetics of the decay phase of the tail currents shows that the decay is evidently slower with a −30 mV than a −60 mV and with a longer (3.3-second) than a short (0.3-second) test pulse. These slower tail currents therefore are unlikely all true tails returning directly from the open to the closed states. The channel must have significantly entered a third gating state, namely the inactivated state (Scheme 1) with a pulse of −30 mV × 0.3 second or −60 mV × 3.3 seconds, and then giving rise to resurgent tail currents upon recovery from state I to state C via state O at −90 mV. In contrast, the inhibition of hERG currents by 10 μM AMD at a test pulse of 0 or +30 mV is manifest with a pulse length of 3.3 but not 0.3 seconds, suggesting that channel activation is no longer significantly slowed, but inactivation is facilitated by AMD at strong depolarization pulses. We have also examined the effect of AMD with lengthening of the test pulse at −60 to −30 mV to 120 seconds (Supplemental Fig. 2). The persistence of the inhibitory effect is consistent with the foregoing ideas that a pulse of −60 mV × 3.3 seconds would already trigger significant channel inactivation and AMD facilitates inactivation. In this regard, it is noted that the time constant of the decay phase of the tail seems to be saturated at ~300 ms (Fig. 1D; Supplemental Fig. 2), signaling the overall kinetics of dissipation of the open state with the I to O and then to C transition (Fig. 1D; Supplemental Fig. 2). The evident inhibitory effect of AMD, however, is also noted on the tail resurgent currents. This could not be envisaged with just slowed activation and/or facilitated inactivation by AMD. AMD very likely has an additional effect on the genesis of the tail resurgent currents, or the recovery process of the inactivated hERG channels upon repolarization (see below).

The Gating Kinetics of hERG Channels Are Markedly Temperature-Dependent. We then compared the hERG cuurents at 37°C and 22°C (Fig. 2). It is evident that the currents are activated much faster at 37°C than at 22°C. hERG channel inactivation, however, does not seem to be accelerated or is even apparently abolished, as there is no discernible decay phase in the macroscopic currents at 37°C. Our data indicate that the biophysical basis of this phenomenon is the slowing of transitions into inactivation (i.e., the C→I and O→I transitions at higher temperature of 37°C). The hERG currents therefore are very much larger at 37°C than at 22°C during a test pulse of either 0.3 or 3.3 seconds, presumably ascribable to not only acceleration of activation but also slowing of the transitions leading to inactivation. In contrast, the tail currents following a short (0.3-second) pulse to −60 mV show a much faster decay phase at 37°C than at 22°C (time constant ~46 vs. ~138 ms). Again, this is probably close to the true tail currents signaling channel deactivation, whose kinetics are therefore evidently temperature-dependent. It is also worthy of note that the time constant of tail current decay is gradually lengthened to ~80 ms with a stronger and/or longer preceding pulse, presumably signaling the change from true deactivating tail to resurgent tail currents (Fig. 2). The lengthening of the time constant in percentage, however, is quantitatively smaller than that in Fig. 1. This is consistent with the idea that hERG channels still undergo inactivation at 37°C, but the tendency of inactivation seems to be decreased. In other words, the steady-state distribution between the open and inactivated states in Scheme 1 is much more in favor of the

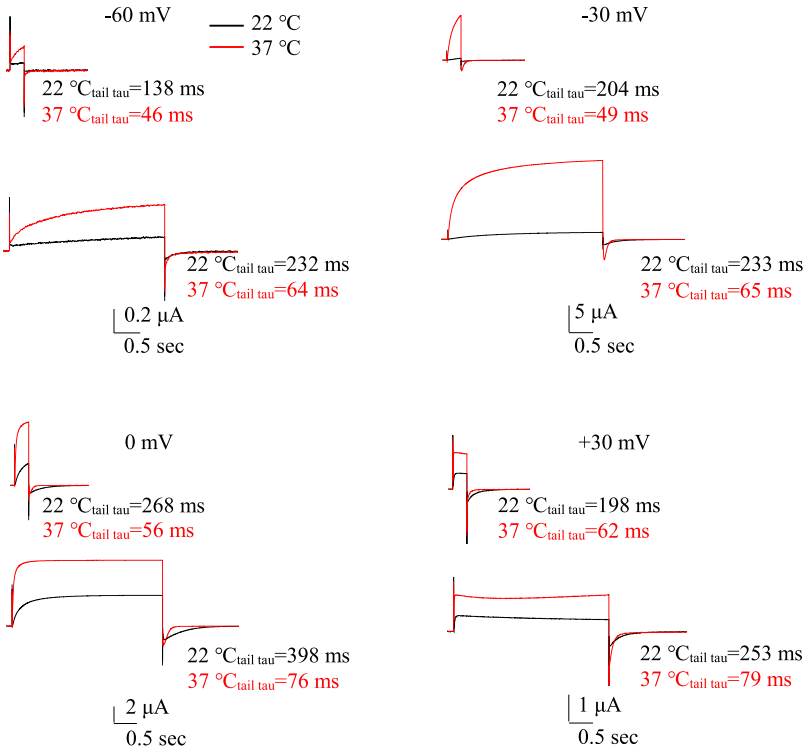

Fig. 2. Temperature dependence of gating kinetics of hERG channels. hERG currents are elicited by the same pulse protocols as that in Fig. 1. Note the much faster activation kinetics and tail current decay (time constants of the decay phases are indicated beside the traces) as well as the much larger current amplitude at 37°C than 22°C. Also note the general lengthening of the time constants of tail current decay with stronger and longer preceding pulses and the possibility of decrease followed by increase of currents during a long and strong pulse (e.g., +30 mV × 3.3 seconds) (data of the same test pulse voltage were acquired from the same cell).

open state at 37°C than at 22°C (see the more complicated and complete gating scheme below), and thus the tail currents may contain a larger true deactivation component of tail currents at 37°C. It is also of note that during a long and strong pulse (e.g., +30 mV × 3.3 seconds), there could be a decrease and then an increase of currents, signaling the possible existence

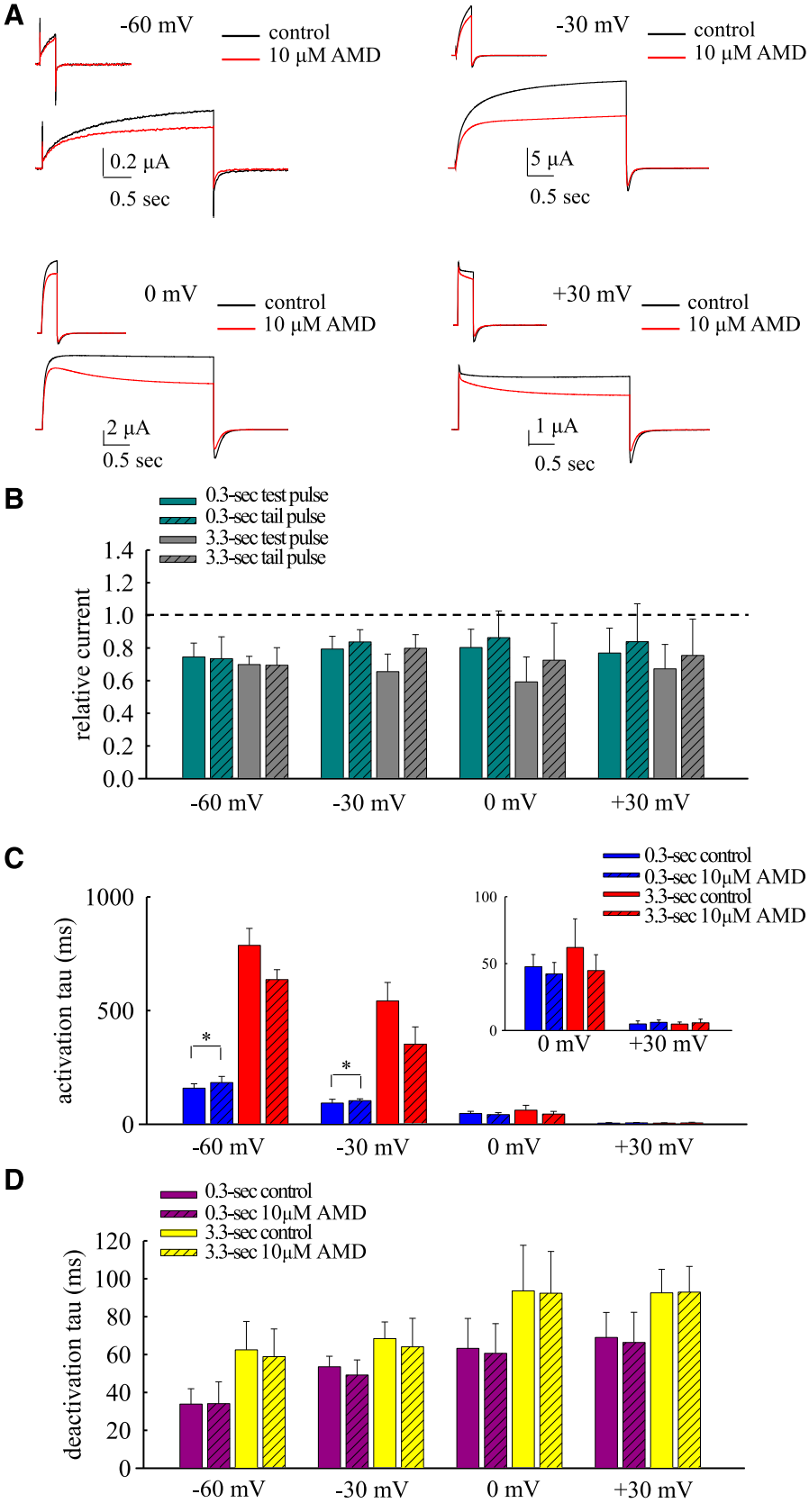

Fig. 3. AMD inhibits hERG currents by enhancement of inactivation at 37°C. (A) hERG currents were elicited by short (0.3-second) and long (3.3-second) test pulses at −60, −30, 0, +30 mV from a holding potential at −90 mV. (B) The late sustained currents (the average currents in the last 5 ms of the test pulse) and the peak of tail currents in 10 μM AMD are normalized to that in control to give the relative currents in the test and tail pulses (0.3 second, green bar; 3.3 seconds, gray bar; n = 10, 10, 11, 10 for −60, −30, −0, +30 mV, respectively). Note the larger current reduction by 10 μM AMD at 0.3-second 0 and +30 mV and the weaker inhibitory effect at 0.3-second −60 and −30 mV than in Fig. 1B (paired two-tailed t test, $P < 0.05$). (C) The time constants from the monoexponential fits to the growing phase of the currents (5% to 95% of currents) in (A) show that 10 μM AMD slows channel activation from holding potential of (−90 mV) at mild pulses (e.g., −60 mV), but not strong pulses (e.g., +30 mV), although the slowing effect is less prominent than that at 22°C in Fig. 1. Also note this is just an approximate estimate of activation kinetics because of the contamination by inactivation (paired two-tailed t test, $^*P < 0.05$). Inset figure: a magnified view of the data at 0 and +30 mV. (D) The time constants from the monoexponential fit to the decay phase of the tail currents (from 5% to 95% of the currents) in (A) show that despite the faster decay kinetics at 37°C, 10 μM AMD has no apparent effect on the deactivation kinetics of hERG currents. Also, more depolarized and prolonged preceding test pulses by themselves still tend to lead to slower decay (longer time constant or τ of the decay phase) of the tail currents. The different pulse durations are indicated by the purple (0.3-second) and yellow (3.3-second) bar, respectively (n = 10, 10, 11, 10 for −60, −30, −0, +30 mV, respectively); data of the same test pulse voltage were acquired from the same cell).

of two different open states with distinct steady-state distribution ratios to their corresponding inactivated states (see below).

AMD Less Effectively Slows hERG Channel Activation but More Effectively Enhances Inactivation at 37°C. Figure 3, A–C, shows that the accelerated hERG channel activation at 37°C is slowed by AMD (most evident in a pulse of −60 to −30 mV, although to a smaller extent than that at 22°C in Fig. 1). Meanwhile, channel inactivation is accentuated by AMD at 37°C (most evident in a pulse of 0 or +30 mV; also see Supplemental Fig. 3). Interestingly, the inhibitory effect on the late sustained current in the test pulse is less and more pronounced in a pulse of −60 to −30 mV and 0 to +30 mV, respectively. Although the decay of the tail currents is much faster at 37°C (and the time constants are gradually lengthened and saturated at ~80 ms), the kinetics of decay again are not changed by AMD (Fig. 3C). Also, AMD still inhibits the tail currents to a similar extent to that of the preceding sustained currents. It seems that AMD has a qualitatively similar action on hERG channels at both 22°C and 37°C. But the quantitative differences, especially those relevant to the pathophysiological and clinical settings, may be worth further exploring.

AMD Binds to the Deactivated hERG Channel with an Apparent Dissociation Constant of ~1.4 μM. We have seen in Supplemental Fig. 2 that 1 to 100 μM AMD concentrations dependently inhibits the currents in a prolonged pulse of −60 to −30 mV × 120 seconds, reasonably approximating a steady-state condition. The IC_{50} is most likely 1 to 3 μM at −60 mV, and probably is higher toward more positive potentials. This is, however, not an ideal estimate of dissociation constant because of the mixture of different gating states of the channel in the long pulse. In view of the apparent effect of AMD on the activation kinetics of the hERG channel, we endeavored to investigate the possibility of AMD binding to the relatively fully deactivated state and thus a more pure gating state of the channel. Figure 4, A and B, and

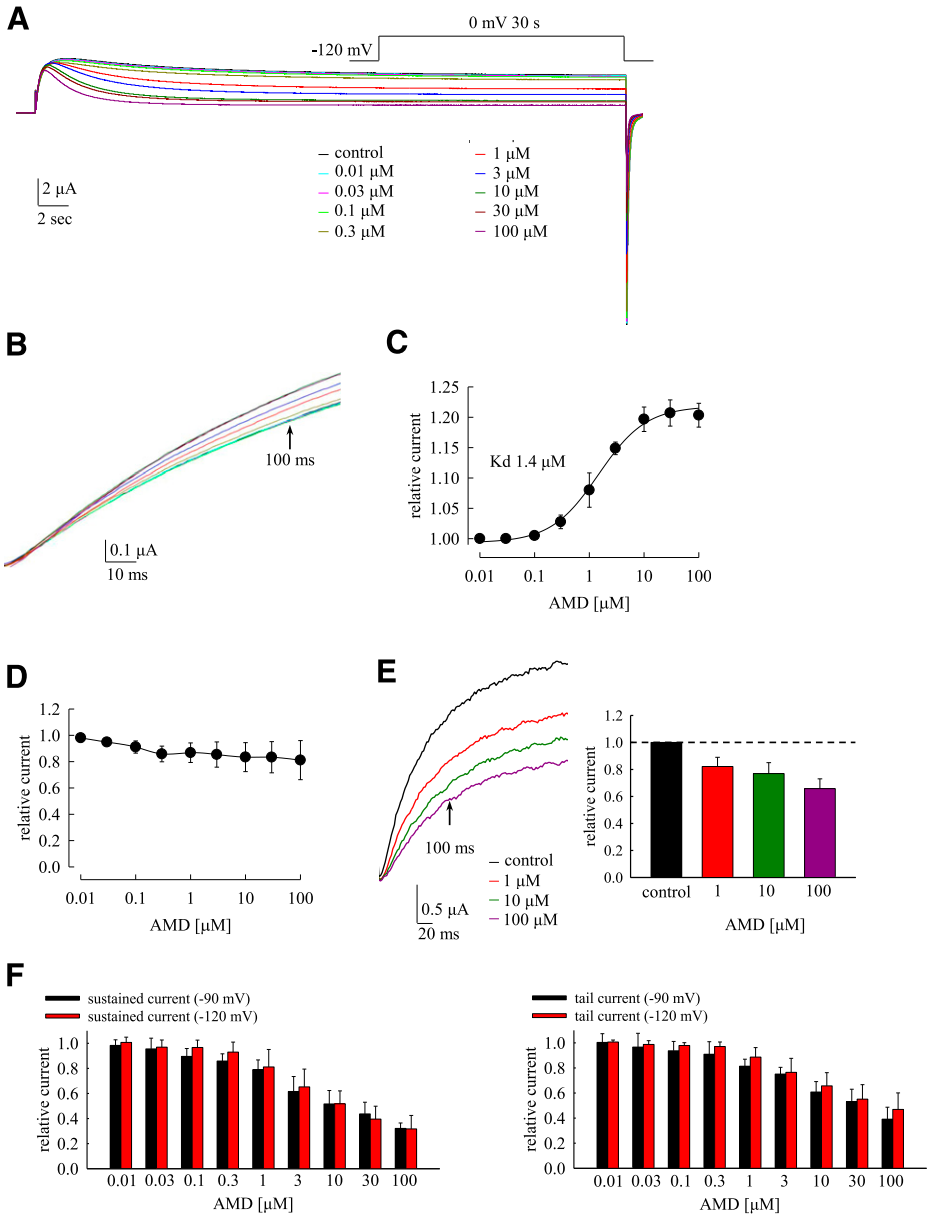

Fig. 4. Concentration-dependent enhancement effect of AMD on the initial activation rate of hERG channels. (A) hERG currents in different concentrations of AMD at 22°C are depicted by different colors. The holding potential is −120 mV, and the test pulse is 0 mV × 30 seconds. The intersweep interval is 1.5 to 3.5 minutes, which is enough to fully recover all inactivated channels back to the resting state. (B) A closer view of the initial activation phase in (A). (C) The current amplitude at 100 ms [arrow in (A)] of the test pulse in different concentrations of AMD is normalized to that in control to give the relative current, which is then plotted against AMD concentration and fitted with a Hill equation to give an apparent K_d value of 1.4 μM (n = 7). (D) With the same test pulse voltage and duration in (A), but a different holding potential at −90 mV, there is no manifest enhancement effect of AMD on the initial phase of channel activation measured in the same way as that in (C) (n = 5). (E) With the same pulse protocol in (A) but at 37°C, the current amplitude at 100 ms (arrow, left panel) is normalized with same procedure in (C) and (D) to give the relative current (right panel). In contrast to the case at 22°C in (B), the initial activation phase is inhibited by AMD at 37°C (n = 4). (F) The late sustained currents (the average currents in the last 5 ms) in the 30-second test pulse (left panel) and the peak of following tail currents (right panel) in AMD with different holding potential (−90 mV vs. −120 mV) are normalized to that in control and plotted against the AMD concentration (red bars: holding potential at −90 mV, n = 5, and black bars: holding potential at −120 mV, n = 7).

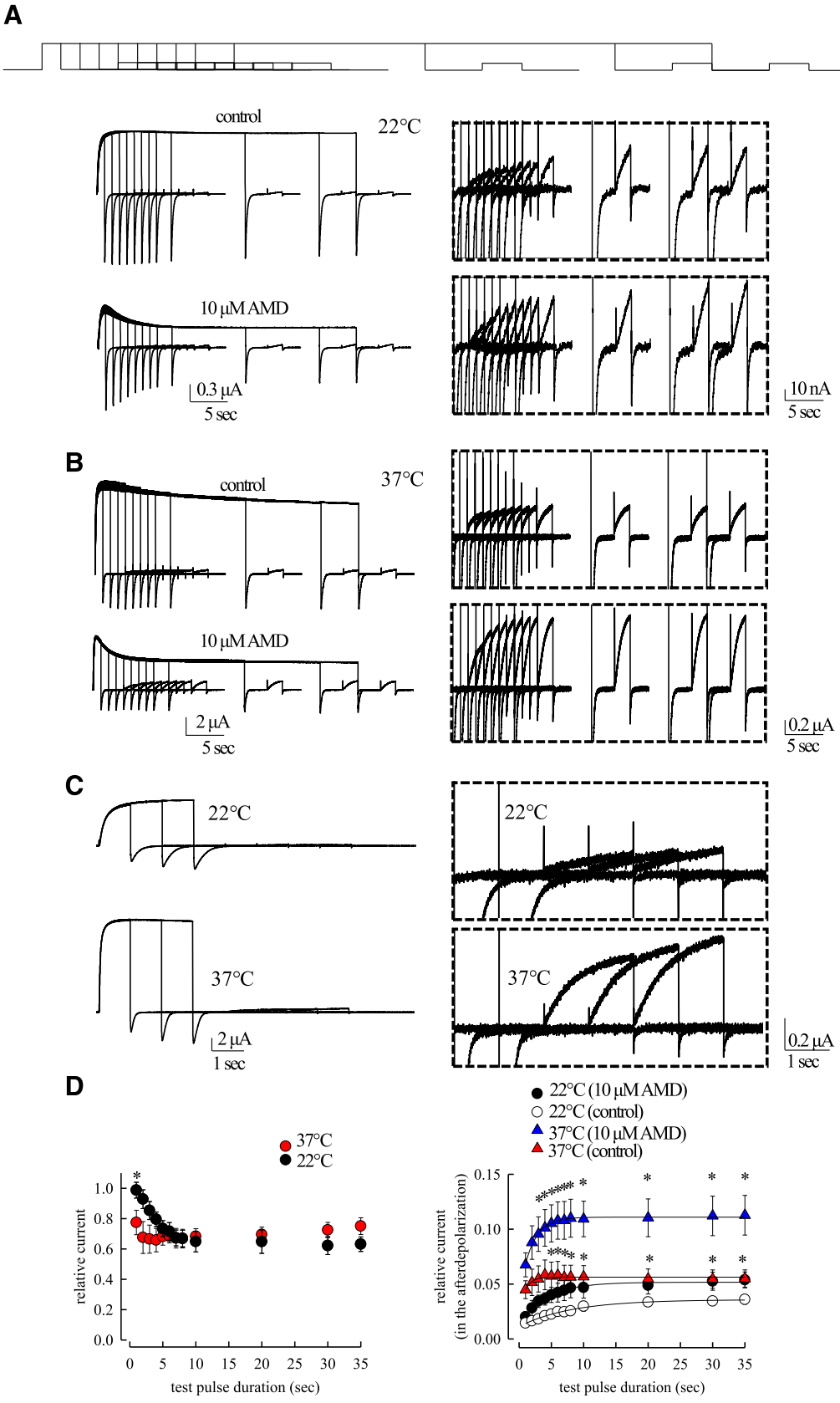

Fig. 5. Inhibition of hERG tail currents and enhancement of the currents in a mild depolarization pulse following a prepulse are dependent on temperature and prepulse duration. (A) Macroscopic current traces were acquired at 22°C with a protocol that a prepulse of 0 mV was lengthened from 1 to 8 seconds ($\Delta t = 1$ second) and then to 10, 20, 30, and 35 seconds from a holding potential of −90 mV. After a gap potential at −90 mV × 3 seconds, a mild depolarization test pulse at −60 mV × 2 seconds (the afterdepolarization) was given before returning back to −90 mV. The intersweep interval is 1.5 to 3.5 minutes, which is enough to fully recover all inactivated channels back to the resting state. The sweeps in control and in 10 μM AMD are shown in the

Supplemental Fig. 4 document the change of activation kinetics, especially the initial kinetics of the hERG by different concentrations of AMD from a holding potential of −120 to 0 mV, which coincides with a narrow window for a protocol to observe acceleration of the initial activation by AMD. Fitting with a one-to-one binding curve to the initial activation kinetics reaction reveals an apparent K_d of ~1.4 μM (Fig. 4C), which could be reasonably ascribed to binding of AMD to the presumably fully deactivated or resting hERG channels (at −120 mV) because the measurement is focused on the initial part of activation. In contrast, the enhancement effect of AMD becomes much less evident when the holding potential is set at −90 mV (Fig. 4D), probably because of the distribution of the channel in less fully deactivated states at the more positive holding potentials and thus more contamination of the activation from the intermediate deactivated states by inactivation. We also repeated the same experiments with a holding potential of −120 mV at 37°C. No enhancement but inhibition or slowing of the initial activation phase was demonstrated (Fig. 4E), presumably because the initial activation from the most deactivated state (at −120 mV) is already quite fast at 37°C. In other words, the apparent enhancement only at 22°C but not 37°C is that the initial activation from −120 mV (presumably from C_1 or the most deactivated state) is already quite fast at 37°C. This is also the reason that there is no apparent enhancement effect even at 22°C if the initial activation is from −90 mV (where channel activation is presumably mostly from C_2 or C_3 rather than C_1 and thus is already accelerated compared with that from −120 mV). In spite of the difference of initial activation phase at holding potential of −90 and −120 mV, the inhibitory effect of AMD on the late currents in the 0 mV pulse or on the tail currents are very similar (Fig. 4F), indicating that the different findings at −90 and −120 mV holding potential are indeed limited to the initial current or channel activation. In any case, AMD seems to bind to the deactivated hERG channel with a binding constant in the low micromolar range, which is well in accordance with the therapeutic concentrations of AMD.

AMD Inhibits Tail hERG Currents by Facilitation of a Silent Route of Recovery from Inactivation. It is well known that hERG channels could recover from inactivation via an open state (e.g., Scheme 1), giving rise to a prominent resurgent tail current. In Figs. 1 and 2, we have seen the evidently smaller resurgent tail currents at 37°C than at 22°C (especially if taking the corresponding sustained currents into consideration). Moreover, the tail resurgent currents are unequivocally inhibited by AMD. The kinetics of tail current decay, however, are not proportionally altered in the presence of AMD. This is very difficult to envisage if AMD only affects hERG channel activation and inactivation. For an explanation of these phenomena, Scheme 1 is inadequate and Scheme 2 is proposed.

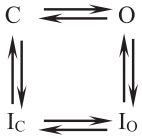

Scheme 2

Scheme 2 indicates at least two possible routes of recovery from inactivation. I_O is the predominant inactivated state during a step depolarization. I_O could recover to state C during the hyperpolarization phase following the step depolarization either via state O (to generate tail or resurgent currents and thus designated as the resurgent route) or via state I_C, which has the activation gate closed before opening of the deinactivation gate and thus would not allow current flow in the recovery processes (the silent route). The inhibition of the resurgent tail currents by AMD therefore is most likely ascribable to facilitation of the silent route of recovery from inactivation, so that the kinetics of tail current decay are unchanged. We therefore explored the recovery from inactivation process in detail. At 22°C, it is evident that the inhibition of tail currents by AMD is more manifest with lengthening of the test pulse (Fig. 5, A and D). Most interestingly, the currents elicited by the following mild pulse at −60 mV (the afterdepolarization) are much larger at 37°C than at 22°C (Fig. 5, B and C), and are further enhanced by AMD (the enhancement effect of AMD is manifest at 22°C, but even more marked at 37°C; Fig. 5D). These features are consistent with the faster channel activation from the intermediate deactivated states at higher temperatures, and thus would make AMD an even better antiarrhythmic at 37°C than at 22°C (see Discussion).

There Are Two Distinct Open and Correlative Inactivated States with Different Propensity for the Silent Route of Recovery. We have seen that AMD facilitates entry into inactivated states as well as silent recovery from inactivation to inhibit hERG currents in different phases. We have also noted that the tail currents either remain at about the same size (Fig. 5B; 37°C) or could be gradually decreased with the lengthening of the prepulse (e.g., Fig. 5A; Supplemental Fig. 5). This is very hard to envisage if there is just one open state (and one directly associated inactivated state) in the gating scheme of hERG channels, in which case the increased inactivation with stronger or longer depolarizing test pulses must be associated with an increase of the resurgent or tail current in the following gap. We therefore propose that there must be at least two distinct open states

upper and lower panels, respectively. The currents in the −60 mV test pulse are magnified in the boxes. Currents were recorded at 22°C in (A) and 37°C in (B). (C) The sample sweeps in (A) and (B) are from different cells. To demonstrate the effect of temperature change itself, we obtained sample sweeps from the same cell at different temperature in the control (drug-free) condition. The pulse protocol was similar to (A), but the prepulse duration was simplified and lengthened from 1 to 3 seconds (Δt = 1 second). Note the enhancement of currents in the prepulse and especially in the afterdepolarization at 37°C. (D) Left panel, the relative (peak) current in the tail pulse in 10 μM AMD is obtained by normalization of the peak tail current in AMD to that in the control to give relative currents, and is also plotted against the test pulse duration (n = 4). The red dot and black dot denoted the results of 37°C and 22°C, respectively. Note the much faster rate of achieving steady-state distribution of the channel to the tail-generating states at 37°C. Right panel, the currents in the −60 mV test pulse are normalized to the sustained current at the end of a prepulse of 35 seconds in control in the same cell to give the relative current, which is then plotted against the prepulse duration and fitted with monoexponential functions (n = 4). The time constants in control and in 10 μM AMD at 37°C are 1.0 and 1.9 seconds, respectively, whereas those at 22°C are 8.2 and 4.2 seconds in control and in 10 μM AMD, respectively. Note the much larger effect of AMD at 37°C than at 22°C (nonpaired one-tailed t test, $^*P < 0.05$).

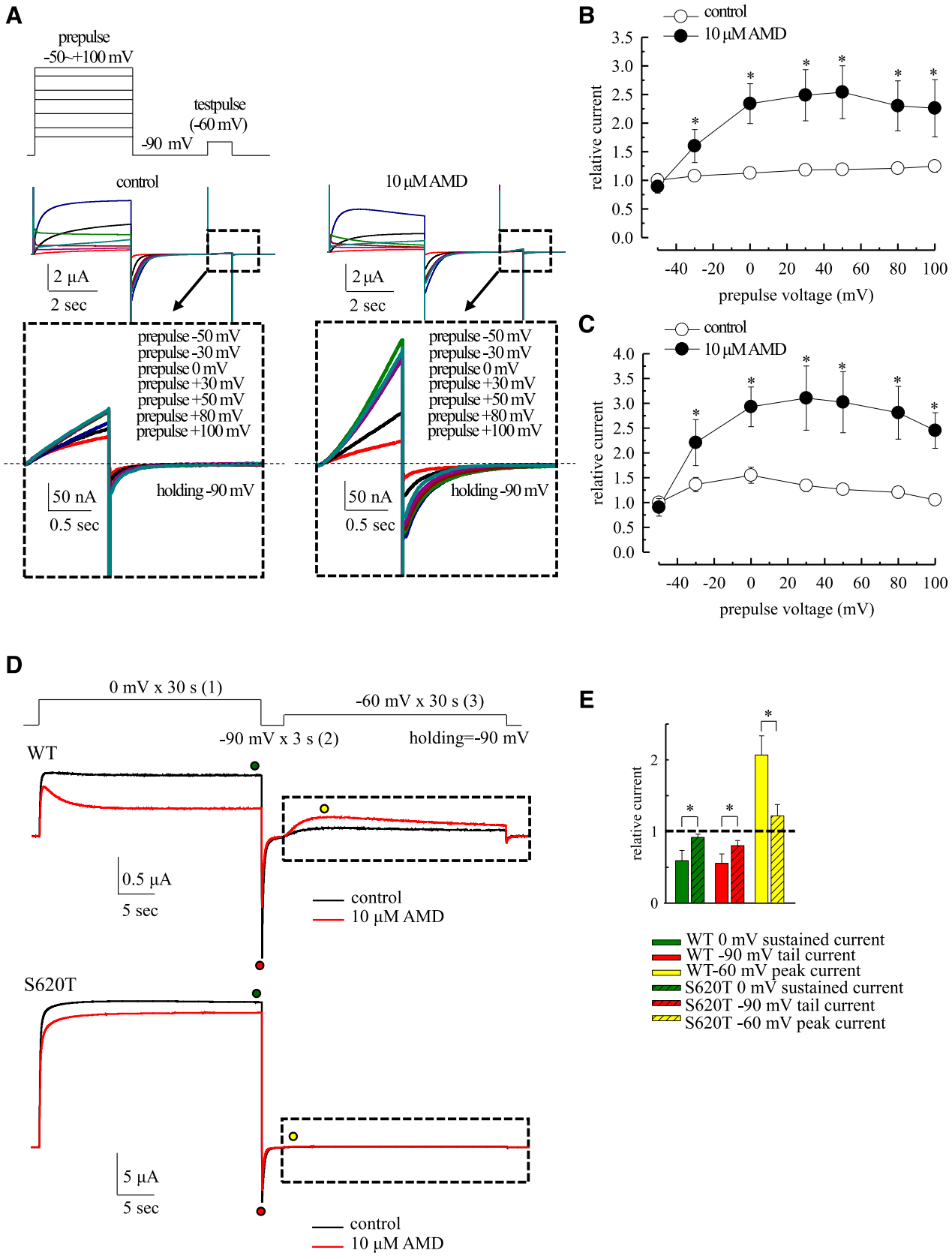

Fig. 6. Voltage dependence of the enhancement effect of AMD on hERG currents in the preceding pulse (prepulse). (A) The prepulses were set to −50 to +100 mV × 4 seconds from a holding potential of −90 mV. The prepulse was followed by a gap (−90 mV × 3 seconds) and then a test pulse (−60 mV × 1 second). Boxes: the hERG currents elicited by the test pulse in control (left) and in 10 μM AMD (right) are magnified. (B and C) The currents elicited by the −60 mV test pulse (part B) and the following tail current at −90 mV (part C) are normalized to those after a prepulse at −50 mV in control in the same cell to give the relative current, which is then plotted against the prepulse voltage (n = 26, 26, 37, 28, 30, 26, and 19 for −50, −30, 0, +30, +50, +80, and +100 mV,

(O_1 and O_2; see Scheme 3 below), each with directly associated inactivated states (I_{O1} and I_{O2}), which have differential propensity of the route of recovery route (Scheme 3, where I_{O1} is more prone to take the silent route of recovery than I_{O2}, but it takes time to reach a steady-state distribution to I_{O1} via O_1, O_2, and I_{O2}).

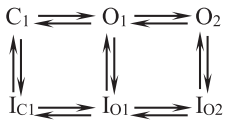

Scheme 3

The transitions between O1 and O2 are further investigated with a strong prepulse at +30 to +60 mV (Supplemental Fig. 5). It is clear that the relative size of tail currents and the gradual decrease of tail currents in AMD are in general much more similar to the case of a prepulse at 0 mV (and 22°C; Fig. 5A). The decrease of tail resurgent currents therefore is correlative to the distribution of channels from I_{O2} to I_{O1}, which could be evidently facilitated by AMD, but not a prepulse of stronger depolarization. The voltage dependence of the transitions between the two open states therefore should be quite lower than C-O or Ic-Io transitions (see Discussion).

AMD Enhances hERG Currents at a Mild Afterdepolarization by Slowing of the Overall Kinetics of Recovery from Inactivation. In Fig. 5, A and B, we have demonstrated that the hERG currents in a mild depolarization following the gap (i.e., afterdepolarization) is enhanced by AMD. Figure 6A examines the possibility in more detail and shows that (at 22°C) the enhancement effect is much more prominent with more depolarized prepulse between −40 and +20 mV, and then reaches a plateau between +20 and +100 mV, consistent with the idea that during the 4-second prepulse, more inactivation channels are generated with a voltage change from −40 to +20 mV, but most channels would have reached the inactivated state at a prepulse potential +20 mV or above. The very similar enhancement effect in Fig. 6, B and C, indicates that it is nearly a true tail or deactivating current following the −60 mV × 1-second afterdepolarization. Moreover, the inactivation-removed S620T mutation also abolishes not only the inhibitory effect of the action of AMD on the current during the step depolarization and the following tail pulse, but also the enhancement effect of AMD on the current during the afterdepolarization (Fig. 6, D and E). It is very interesting that AMD should markedly inhibit hERG currents elicited by a −60 mV pulse if there are no preceding pulses (e.g., Figs. 1 and 3; Supplemental Fig. 3), but markedly enhances the currents if there is a preceding pulse resulting in significant channel inactivation. It is plausible that the direct cause of the enhancement effect is activation of hERG channels not from the fully but from the intermediate deactivated states because the intervening gap is not long enough to allow a full recovery process (recovery back to the fully deactivated state), and AMD further slows this recovery process. Supplemental Fig. 6 shows that the enhancement effect is in general larger in the presence of AMD, and gets smaller with lengthening of the gap. Moreover, the decay of the enhancement effect is markedly slower in AMD than in control (time constants 43.8–45.7 seconds in AMD vs. 11.6–19.8 seconds in control at a holding potential of −90 mV; Supplemental Fig. 6), well substantiating the idea of slower recovery from inactivation (thus less propensity to stay in the fully deactivated state with a limited length of gap and consequently more activation at the subsequent afterdepolarization) in AMD. In other words, more hERG channels would be in the intermediate closed states with a relatively short recovery period after a prepulse (Scheme 4, where C_2 is the intermediate closed or deactivated state, and C_1 is the fully deactivated state; I_{C2} and I_{C1} are the deactivated and also inactivated states corresponding to C_2 and C_1, respectively).

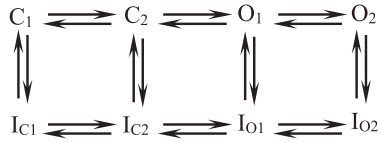

Scheme 4

hERG channels are therefore more easily activated or enhanced by an afterdepolarization, if the depolarization is not so widely separated from the previous one (i.e., if the depolarization is an afterdepolarization). This would be especially true at 37°C, where channel activation is itself much faster than at 22°C, and again could be a major advantage against premature afterdepolarization in the genesis of cardiac arrhythmias especially at 37°C (see Discussion).

AMD Shows Temperature-Dependent and Use-Dependent Modification Effect on hERG Currents in Pulse Protocols Simulating Normocardia and Tachycardia. With pulse protocols simulating normocardia and tachycardia (Fig. 7), it is clear that inhibition of hERG currents by AMD during the depolarization prepulse and the following gap (i.e., tail resurgent currents) are both use-dependent, although it is definitely faster to achieve the steady-state effect at 37°C than 22°C and at 1.67 Hz than 1.11 Hz. Because the cardiac plateau potential is characterized by short (~300 ms in length) and strong (0 to +30 mV) depolarization, and the interpulse interval (the repolarization interval) between two plateaus is only a few hundred milliseconds in physiologic conditions, the inactivated channels may accumulate with repeated pulses to make the use dependence. The inhibition of hERG currents during the depolarization prepulses and the intervening repolarization steps (i.e., the tail currents) are more pronounced at 37°C than 22°C in most cases (see also Fig. 1B; Fig. 3B; Supplemental Fig. 3). The plateau-prolongation effect of AMD

respectively, paired one-tailed t test, $^*P < 0.01$). The lines between the data points are drawn by hand. (D) The effect of 10 μM AMD on the S620T mutant channel. The pulse protocol is characterized by a holding potential at −90 mV, and two pulses to 0 mV for 30 seconds and to −60 mV for 30 seconds with an intervening gap at −90 mV for 3 seconds. The sample currents in the wild-type (upper panel) and the S620T mutant channels (lower panel) are shown. (E) The late sustained currents at 0 mV (green circle), the peak tail currents at −90 mV (red curcle), and the peak currents at −60 mV (yellow circles) in 10 μM AMD are normalized to that in control in the same cell to give the relative current (shown in bars color coded to the circles). Note the much smaller effect of AMD in the mutant than in the wild-type channels (all $n = 5$, nonpaired two-tailed t test, $^*P < 0.01$).

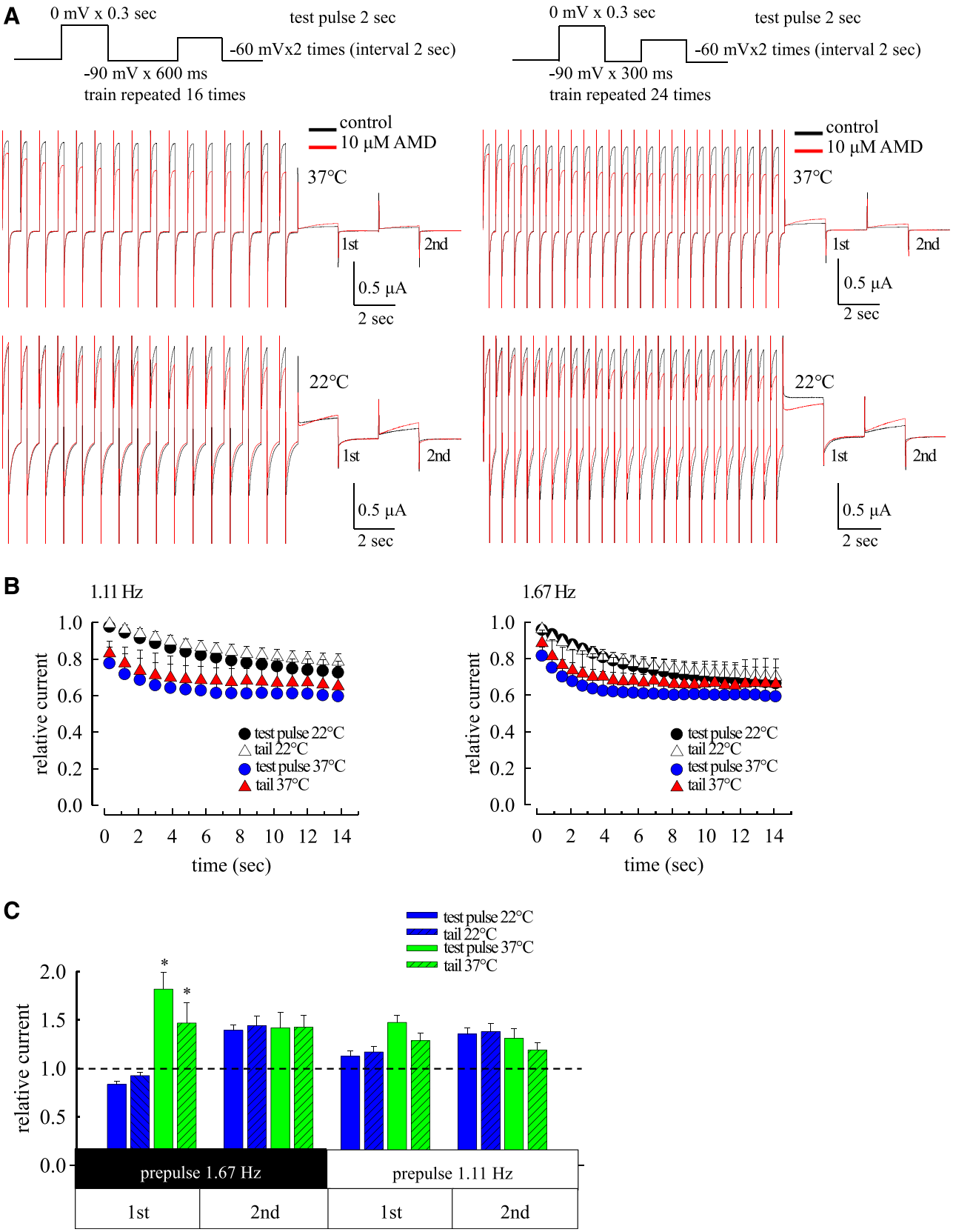

Fig. 7. Use-dependent inhibition and enhancement effect of AMD on hERG currents with pulse protocols simulating normocardia and tachycardia at 22°C or 37°C. (A) Left panel: hERG currents were elicited by prepulses (0 mV × 300 ms) repeated at 1.11 Hz to mimic the cardiac rhythms in normocardia. The intervening repolarization phase between two prepulses was set to −90 mV × 600 ms. The 16 repeated prepulses were followed by two test pulses (−60 mV × 2 seconds, labeled as first and second) with an intervening interval of 2 seconds. The holding potential was −90 mV. Right panel: hERG currents were elicited by the same pulse protocols as that in the left panel except that the intervening repolarization phase between the prepulse is shortened to 300 ms (so that the prepulses were repeated at 1.67 Hz to mimic mild tachycardia). (B) The relative current (current in AMD/current in

therefore is very likely dependent on the temperature and cardiac rhythms at least within a feasible range. The inhibition of tail currents by AMD would in theory slightly decrease the assurance of a rapid and relatively undisturbed repolarization phase once the plateau phase is over and membrane repolarization ensues (see Discussion). In this regard, the hERG currents elicited by afterdepolarization −60 mV after the foregoing repeated pulses are markedly enhanced rather than inhibited by AMD (see also Figs. 5 and 6; Supplemental Fig. 6). This effect is well more pronounced with tachycardia than normocardia, and at 37°C than 22°C. Many more hERG currents are thus available to counteract the afterdepolarization or premature beat in the presence of AMD especially for a condition of tachycardia or tachyarrhythmia at 37°C (i.e., more use-dependent enhancement of hERG currents of AMD during an early or delayed afterdepolarization following a repolarization phase; see Discussion).

Discussion

The Characteristics of hERG Channel Gating: The Versatile Routes of Development of and Recovery from Inactivation in Terms of Trespassing the Open States. hERG channels are well known for their faster inactivation than activation kinetics (at relative strong depolarization pulses) and the occurrence of resurgent tail currents upon repolarization (i.e., recovery from inactivation via the resurgent route) (Vandenberg et al., 2004). The former could be readily envisaged with the relatively enhanced C→I transitions than C→O transitions in Fig. 8. The molecular routes of recovery from inactivation have not been fully characterized, although it has been inferred that hERG channels may be inactivated or recover from inactivation without trespassing the open state (Luo and Rudy, 1994; Clancy and Rudy, 2001; Lu et al., 2001). We demonstrate that, in contrast to the resurgent route of recovery where the inactivation gate reopens before the closure of the activation gate and an open state is therefore trespassed, there is a silent route of recovery where the inactivation gate reopens after the closure of the activation gate (Cuello et al., 2010; Perry et al., 2013) (see the gating scheme in Fig. 8; the I_{O2} to I_{O1} to I_5 transitions embody the silent route, and the I_{O2} to O_2, or I_{O1} to O_1, and then to C_5 transitions embody the resurgent route). The existence of the silent route of recovery necessarily argues for direct connections between the closed and inactivated states, or channel inactivation without trespassing the open state, which is consistent with the aforementioned explanation for the faster inactivation than activation at strong depolarization, and could also play an imperative role in the understanding of the action of AMD. In other words, this could be part of the reason that hERG currents are so much decreased without so much apparent increase in the macroscopic inactivation kinetics at strong depolarization because many channels are directly distributed to multiple intermediate closed and then multiple intermediate inactivated states from the closed states. Based on the simulation results in Fig. 8, we found that most inactivated hERG channels actually recover via the silent route. However, the small proportion going through the resurgent route is sufficient to give rise to sizable tail currents. The inactivation under consideration in this case presumably is the C-type inactivation (Schönherr and Heinemann, 1996; Wang et al., 1997; Torres et al., 2003; Jiang et al., 2005), which is ascribable to conformational changes in the external pore vestibule. Cations or drugs binding to this external pore region have been reported to have a prominent effect on the movement of voltage sensors in the K^+ or Na^+ channel (Liu et al., 1996; Smith et al., 1996; Jiang et al., 1999; Yang and Kuo, 2002; Milnes et al., 2003; Mitcheson, 2003; Kuo et al., 2004; Zhang et al., 2004; Yang and Kuo, 2005; Yang et al., 2009; Catterall, 2010) and thus the voltage dependence of a molecular behavior. The conformational changes at the internal and external pore mouths (responsible for activation and C-type inactivation, respectively) may directly interact with each other via a recess-like structure in the pore (e.g., the S6 recess) (Yang et al., 2009) skipping the selectivity filter. The activation–inactivation coupling therefore could be established either via the movement of the voltage sensors indirectly or more direct local interactions involving the S6 recess or relevant structure. The complex gating processes, or more precisely the very versatile voltage dependence as well as molecular routes of activation/inactivation and recovery from inactivation of hERG channels, may thus involve many different (internal, external, and transmembrane) parts of the channel protein. This could be the reason that hERG channels are so vulnerable to different kinds of pharmacological and toxicological modulations.

The Molecular Actions of AMD on hERG Channels: Increased Voltage Dependence of Activation/Inactivation and Facilitated Silent Recovery from Inactivation Especially at 37°C. We have shown that AMD binds to the deactivated channel with an apparent dissociation constant of 1.4 μM, well within the clinical therapeutic range of the drug. We have also shown that hERG channel activation is slowed by AMD at mild (i.e., −60 to −30 mV) but not strong depolarization (i.e., 0 to +30 mV), where a more prominent macroscopic inactivation may also be observed. It is plausible that in clinical settings AMD would already bind to most deactivated hERG channels to increase the voltage dependence of channel activation and/or inactivation. In other words, there is likely more charge movement between −30 and 0 mV with AMD binding. Because of the faster activation and inactivation kinetics at 37°C than 22°C, it is especially of note that the foregoing pharmacological attributes are sensitive to temperature. The inhibitory effect of AMD on the hERG currents is thus decreased during mild depolarization but increased at stronger depolarization at 37°C (Figs. 1 and 3; Supplemental Fig. 3), making AMD an even better antiarrhythmic for tachyarrhythmia at the body than room temperature (by lengthening the plateau potential, which usually reaches 0 mV or above). In addition to the foregoing changes in the development of activation and inactivation, AMD also affects the recovery process from inactivation by facilitation of the silent route of recovery from inactivation. AMD therefore tends to inhibit the tail currents by shifting the distribution to the

control) during the prepulses and the following tail phases are plotted against the elapsed time (left panel, 1.11 Hz; right panel, 1.67 Hz). (C) Currents in the first and second test pulses to −60 mV in the presence of AMD are normalized to that in control to give the relative current. Note that AMD has the strongest enhancement effect for the first test pulse at 37°C (all $n = 4$, nonpaired two-tailed t test, $^*P < 0.01$).

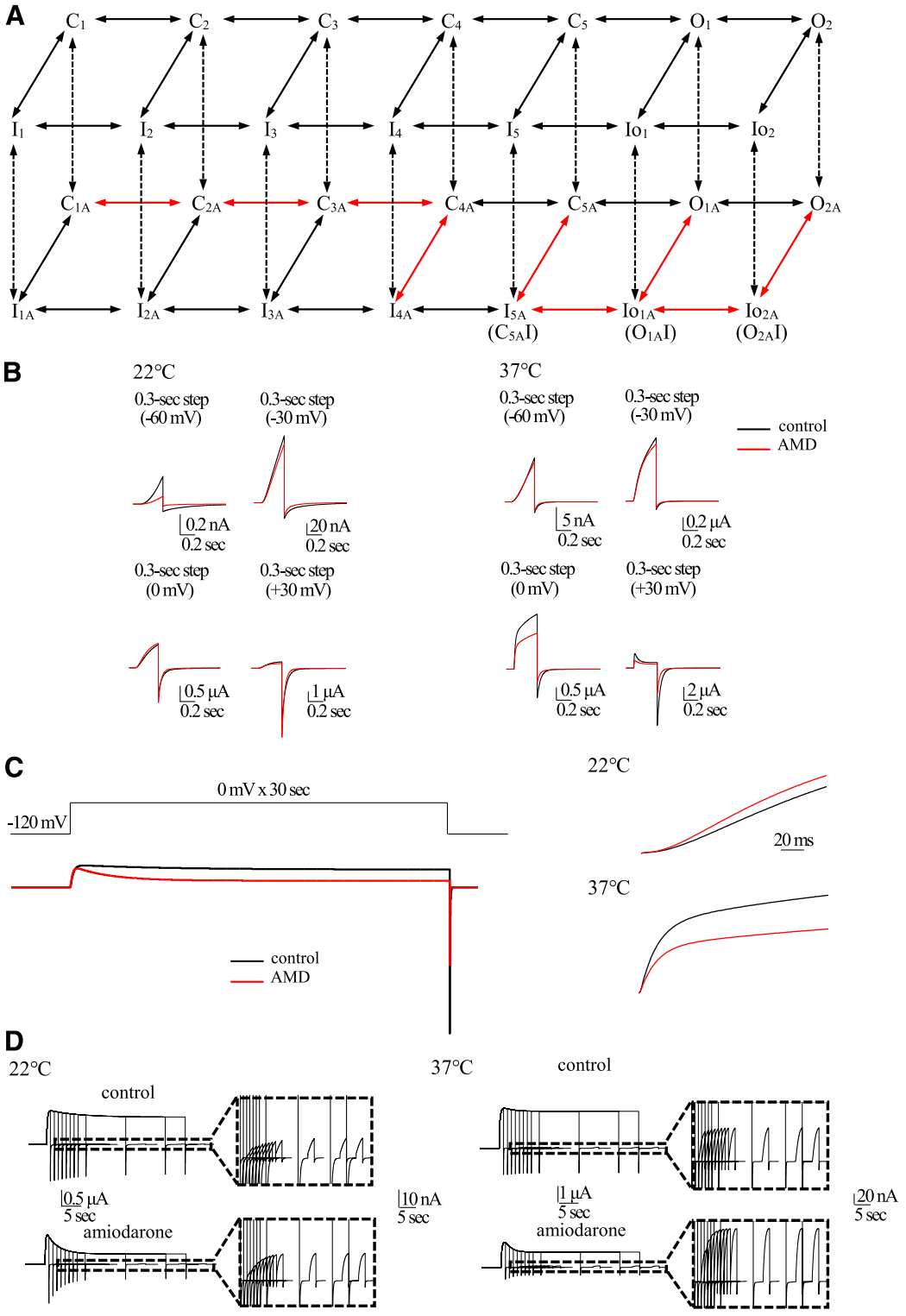

Fig. 8. A gating scheme of the hERG channel and simulation of hERG currents in control and in AMD at 37°C than 22°C. (A) The 14 states in the upper panel are for the control condition, and the 14 states in the lower panel are AMD-bound and stand for the gating processes in the presence of AMD. The two sets of kinetic parameters at 22°C are provided in Table 1, based on which the currents at 22°C and 37°C are calculated. Note that the transitions leading into the inactivated states tend to be slower (i.e., lower K_0 values) at 37°C, demonstrating the decreased inactivation at 37°C than 22°C (Figs. 1 and 3). Also note that the voltage dependence of the C-C transitions is in general higher in AMD than in control (Fig. 1), and that the voltage dependence of the transitions between the two open states is in general lower than the C-O transitions (Fig. 5; Scheme 3). The state-dependent binding and unbinding rates of AMD (indicated by the vertical dotted arrows) are not modeled for the sake of simplicity. This is a reasonable approximation because in therapeutic conditions the free concentrations of AMD (~3 μM) shall be well above the dissociation constants of AMD binding to the deactivated channels (Fig. 4). There are two open states (O_1 and O_2). At mild pulses most of hERG channels will enter the first O_1 state and then the I_{O1} state, the recovery from which would trespass either O_1 (i.e., the resurgent route for the generation of the tail currents) or I_5 (the silent route). At stronger and longer depolarization, the channel would be distributed more and more to states O_2 and I_{O2} than states O_1 and I_{O1}. The recovery from I_{O2} would tend to generate larger tail because of the higher rate of $I_{O2} \rightarrow O_2$ than $I_{O1} \rightarrow O_1$, and also because even if the channel takes the $I_{O2} \rightarrow I_{O1}$ route, it can still have another chance

TABLE 1

Kinetic parameters for hERG channel gating in control and presented of AMD at 22°C and 37°C

Voltage-dependent rates are expressed as $k_{(v)} = k_0 \exp(k_1 V)$, where $k_{(v)}$ stands for the transitional rate at a designated membrane potential V (in millivolts) at 22°C. Transitions with negligible transitioned rates (i.e., zero) are not indicated here for the sake of simplicity. For the electronic charge displacement during activation, please also refer to the single unit of voltage sensors movement in previous hERG models (Johnson et al., 1999; Bett et al., 2011). The values are based on the root template (22°C), and each transition of the conditions at 37°C is given. The changes in voltage dependence of activation ($C_1 \leftrightarrow C_2 \leftrightarrow C_3 \leftrightarrow C_4$) by AMD are based on the experiments in Figs. 1 and 3. The increase of silent route for entry to and recovery from inactivation by AMD ($I_{O2} \rightarrow I_{O1}$, $I_{O1} \rightarrow I_5$) is based on the experiments in Fig. 5. The slowing of transitions into inactivation (C→I and O→I) at higher temperatures, and the increase of voltage dependency of inactivation (C→I and O→I) when in the presence of AMD are based on the experiments in Figs. 1–3 and 5. The major changes made by AMD are shown in bold.

	Control			Amiodarone	
	k_0 (ms^{-1})	k_1 (mV^{-1})		k_0 (ms^{-1})	k_1 (mV^{-1})
C_1C_2	$2.96_{(22°C)}$ vs. $5.437867_{(37°C)}$	0.146	$C_{1A}C_{2A}$	$2.96_{(22°C)}$ vs. $5.437867_{(37°C)}$	**$0.155_{(22°C)}$ vs. $0.148_{(37°C)}$**
C_2C_3	$0.71821_{(22°C)}$ vs. $0.944112_{(37°C)}$	$0.049_{(22°C)}$ vs. $0.0265_{(37°C)}$	$C_{2A}C_{3A}$	$0.71821_{(22°C)}$ vs. $0.944112_{(37°C)}$	**$0.059_{(22°C)}$ vs. $0.009_{(37°C)}$**
C_3C_4	$0.55821_{(22°C)}$ vs. $1.698739_{(37°C)}$	$0.002_{(22°C)}$ vs. $0.001_{(37°C)}$	$C_{3A}C_{4A}$	$0.55821_{(22°C)}$ vs. $1.698739_{(37°C)}$	**$0.005_{(22°C)}$ vs. $0.001_{(37°C)}$**
C_4C_5	$0.035321_{(22°C)}$ vs. $0.348799_{(37°C)}$	0.001	$C_{4A}C_{5A}$	$0.035321_{(22°C)}$ vs. $0.348799_{(37°C)}$	0.001
C_5O_1	$1.05E{-}5_{(22°C)}$ vs. $4.7E{-}5_{(37°C)}$	0.001	$C_{5A}O_{1A}$	$1.05E{-}5_{(22°C)}$ vs. $4.96E{-}5_{(37°C)}$	0.001
O_1O_2	$0.02545_{(22°C)}$ vs. $0.029361_{(37°C)}$	0.00071547	$O_{1A}O_{2A}$	0.02863	0.00071547
C_2C_1	$0.00001_{(22°C)}$ vs. $0.000015_{(37°C)}$	−0.07966	$C_{2A}C_{1A}$	$0.00001_{(22°C)}$ vs. $0.000033_{(37°C)}$	−0.07966
C_3C_2	$0.6_{(22°C)}$ vs. $0.889337_{(37°C)}$	−0.00166	$C_{3A}C_{2A}$	$0.6_{(22°C)}$ vs. $1.957876_{(37°C)}$	−0.00166
C_4C_3	$1.2_{(22°C)}$ vs. $2.204541_{(37°C)}$	−0.00166	$C_{4A}C_{3A}$	$1.2_{(22°C)}$ vs. $3.142763_{(37°C)}$	−0.00166
C_5C_4	$1.8_{(22°C)}$ vs. $3.989752_{(37°C)}$	−0.04366	$C_{5A}C_{4A}$	$1.8_{(22°C)}$ vs. $3.989752_{(37°C)}$	−0.04366
O_1C_5	$0.00055_{(22°C)}$ vs. $0.000602_{(37°C)}$	−0.04158	$O_{1A}C_{5A}$	$0.00055_{(22°C)}$ vs. $0.000802_{(37°C)}$	−0.04158
O_2O_1	$0.12_{(22°C)}$ vs. $0.424824_{(37°C)}$	−0.08158	$O_{2A}O_{1A}$	$0.1651_{(22°C)}$ vs. $0.24445_{(37°C)}$	−0.08158
C_4C_3	$1.2_{(22°C)}$ vs. $2.2045401_{(37°C)}$	−0.00166	$C_{4A}C_{3A}$	$1.2_{(22°C)}$ vs. $3.142763_{(37°C)}$	−0.00166
C_3C_2	$0.6_{(22°C)}$ vs. $0.889337_{(37°C)}$	−0.00166	$C_{3A}C_{2A}$	0.6 vs. $1.957876_{(37°C)}$	−0.00166
C_2C_1	$0.00001_{(22°C)}$ vs. $0.000015_{(37°C)}$	−0.07966	$C_{2A}C_{1A}$	0.00001 vs. $0.000033_{(37°C)}$	−0.07966
I_1I_2	$0.011_{(22°C)}$ vs. $0.020208_{(37°C)}$	0.146	$I_{1A}I_{2A}$	0.011 vs. $0.01446_{(37°C)}$	$0.155_{(22°C)}$ vs. $0.148_{(37°C)}$
I_2I_3	$0.011_{(22°C)}$ vs. $0.01446_{(37°C)}$	$0.049_{(22°C)}$ vs. $0.0265_{(37°C)}$	$I_{2A}I_{3A}$	0.011 vs. $0.020208_{(37°C)}$	$0.059_{(22°C)}$ vs. $0.009_{(37°C)}$
I_3I_4	$0.00011_{(22°C)}$ vs. $0.000335_{(37°C)}$	$0.002_{(22°C)}$ vs. $0.001_{(37°C)}$	$I_{3A}I_{4A}$	0.00011 vs. $0.000335_{(37°C)}$	$0.005_{(22°C)}$ vs. $0.001_{(37°C)}$
I_4I_5	$0.0128_{(22°C)}$ vs. $0.018973_{(37°C)}$	0.001	$I_{4A}I_{5A}$	0.01392 vs. $0.020633_{(37°C)}$	0.001
I_5I_{O1}	$0.068188_{(22°C)}$ vs. $0.078668_{(37°C)}$	0.001	$I_{5A}I_{O1A}$	0.07127 vs. $0.130931_{(37°C)}$	0.001
$I_{O1}I_{O2}$	$0.073695_{(22°C)}$ vs. $0.085021_{(37°C)}$	0.00071547	$I_{O1A}I_{O2A}$	0.1126	0.00071547
$I_{O2}I_{O1}$	$0.83054_{(22°C)}$ vs. $2.448496_{(37°C)}$	−0.08158	$I_{O2A}I_{O1A}$	**$1.265_{(22°C)}$ vs. $3.74082_{(37°C)}$**	−0.08158
$I_{O1}I_5$	$0.069357_{(22°C)}$ vs. $0.129264_{(37°C)}$	−0.04158	$I_{O1A}I_{5A}$	**$0.079857_{(22°C)}$ vs. $0.173907_{(37°C)}$**	−0.04158
I_5I_4	$0.061484_{(22°C)}$ vs. $0.09195_{(37°C)}$	−0.04366	$I_{5A}I_{4A}$	$0.065484_{(22°C)}$ vs. $0.09195_{(37°C)}$	−0.04366
I_4I_3	$0.000042_{(22°C)}$ vs. $0.000059_{(37°C)}$	−0.00166	$I_{4A}I_{3A}$	$0.00035_{(22°C)}$ vs. $0.000524_{(37°C)}$	−0.00166
I_3I_2	$2.0e{-}9_{(22°C)}$ vs. $2.96446E{-}9_{(37°C)}$	−0.00166	$I_{3A}I_{2A}$	$2.0E{-}9_{(22°C)}$ vs. $6.526254E{-}9_{(37°C)}$	−0.00166
I_2I_1	$2.0e{-}9_{(22°C)}$ vs. $2.96446E{-}9_{(37°C)}$	−0.07966	$I_{2A}I_{1A}$	$2.0E{-}9_{(22°C)}$ vs. $6.526254E{-}9_{(37°C)}$	−0.07966
C_4I_4	$0.0232_{(22°C)}$ vs. $0.0106_{(37°C)}$	0.039942	$C_{4A}I_{4A}$	$0.03215_{(22°C)}$ vs. $0.0111_{(37°C)}$	**0.0451**
C_5I_5	$0.0369_{(22°C)}$ vs. $0.025_{(37°C)}$	0.039942	$C_{5A}I_{5A}$	$0.0479_{(22°C)}$ vs. $0.0285_{(37°C)}$	**0.0451**
O_1I_{O1}	$0.492_{(22°C)}$ vs. $0.055_{(37°C)}$	0.039942	$O_{1A}I_{O1A}$	$0.492_{(22°C)}$ vs. $0.055_{(37°C)}$	**0.0451**
O_2I_{O2}	$0.8_{(22°C)}$ vs. $0.2_{(37°C)}$	0.039942	$O_{2A}I_{O2A}$	$0.8_{(22°C)}$ vs. $0.2_{(37°C)}$	**0.0451**
I_4C_4	$3.80E{-}5_{(22°C)}$ vs. $1.70889e{-}5_{(37°C)}$	$-0.048_{(22°C)}$ vs. $-0.075_{(37°C)}$	$I_{4A}C_{4A}$	$3.75E{-}5_{(22°C)}$ vs. $4.9295E{-}5_{(37°C)}$	$-0.048_{(22°C)}$ vs. $-0.075_{(37°C)}$
I_5C_5	$3.80E{-}5_{(22°C)}$ vs. $1.70889e{-}5_{(37°C)}$	$-0.048_{(22°C)}$ vs. $-0.075_{(37°C)}$	$I_{5A}C_{5A}$	$3.75E{-}5_{(22°C)}$ vs. $4.9295E{-}5_{(37°C)}$	$-0.048_{(22°C)}$ vs. $-0.075_{(37°C)}$
$I_{O1}O_1$	$3.80E{-}5_{(22°C)}$ vs. $1.70889E{-}5_{(37°C)}$	$-0.048_{(22°C)}$ vs. $-0.075_{(37°C)}$	$I_{O1A}O_{1A}$	$3.75E{-}5_{(22°C)}$ vs. $4.9295E{-}5_{(37°C)}$	$-0.048_{(22°C)}$ vs. $-0.075_{(37°C)}$
$I_{O2}O_2$	$0.0001056_{(22°C)}$ vs. $0.000139_{(37°C)}$	$-0.048_{(22°C)}$ vs. $-0.075_{(37°C)}$	$I_{O2A}O_{2A}$	$0.0001188_{(22°C)}$ vs. $0.0001562_{(37°C)}$	$-0.048_{(22°C)}$ vs. $-0.075_{(37°C)}$

inactivated state with a higher likelihood propensity to recover from inactivation via the silent route (e.g., I_{O1} in Fig. 8). Moreover, the inhibitory effect of AMD of the tail currents is stronger at 37°C by AMD (with a physiological pulse protocol; Fig. 7B), again making AMD a better antiarrhythmic for tachyarrhythmia at the body temperature because of the stronger prolongation effect on the repolarization phase (phase 3) in the cardiac action potential (see below). It is conceivable that AMD does not significantly jeopardize ion conduction, but deters the initial outward movement of the voltage sensors and the reopening of the C-type inactivation gate. The local electrical field is more condensed, however, so that the same movement of the voltage sensor now embodies a larger electrical energy change. The activation rate at mild depolarization is therefore slowed, but the activation as well as inactivation rates are more accelerated at stronger depolarization, by AMD. By the same token, AMD may also facilitate the silent route but slows the overall kinetics of recovery from inactivation with the altered electrical field and/or microenvironment of the voltage sensors and thus the electrical as well as nonelectrical energy changes associated with gating (see the gating scheme in Fig. 8).

The Unique Effect of AMD against Tachyarrhythmia: Different Use-Dependent and Temperature-Dependent Inhibition and Enhancement of hERG Currents at Different Phases of Cardiac Action Potentials. We have seen that the inhibition of hERG currents by AMD during the test and tail pulses is more pronounced and develops faster with more frequently repetitive pulses and higher temperature (Fig. 7). AMD therefore would necessitate less use or fewer

of choosing the resurgent route of recovery from O_1. AMD not only increases channel activation/inactivation at moderate depolarization, but would also increase the relative proportion of $I_{O2} \rightarrow I_{O1} \rightarrow I_5$ so that there are decreasing tail currents associated with increased inactivation. These major changes made by AMD are shown in red arrows. (B) Simulation of the currents elicited by (−60, −30, 0, and +30 mV) with short (300-ms) depolarization pulse (the same as that in Figs. 1 and 3). (C) Simulation of the currents with the same protocols in Fig. 4. Note enhancement and inhibition of the currents in the initial activation phase by AMD at 22°C and 37°C, respectively. (D) Simulation of the currents with the same protocols in Fig. 5. Note enhancement of the currents in the afterdepolarization (at −60 mV) by AMD especially at 37°C.

repetitive plateau depolarization pulses at 37°C to achieve an adequate inhibition of hERG currents during the plateau depolarization (Sager et al., 1993). The inhibition of hERG tail currents by AMD also contributes to a prolonged repolarization phase following the depolarization and thus a slower and normalized heart rate. Most interestingly, if any perturbation of the membrane potential should happen during the repolarization phase and lead to premature depolarization (i.e., afterdepolarization), more hERG currents would be elicited to counteract the premature depolarization in the presence of AMD especially in a condition of tachycardia and especially at 37°C (i.e., use-dependent inhibition of hERG currents at the preceding plateau and use-dependent enhancement of hERG currents at the afterdepolarization; Fig. 7). AMD therefore is a unique pharmacological agent, effectively lengthening the plateau and repolarization phase of the cardiac action potential to ameliorate tachycardia on the one hand, and effectively protecting the repolarization phase from premature afterdepolarization on the other hand to assure low risk of tachyarrhythmia. The hallmark of type III antiarrhythmic agents is inhibition of the K^+ channels and thus prolongation of the QT interval, which has direct slowing effect on tachycardia. The inhibition of K^+ channels, however, increases the chances of early and delayed afterdepolarization and thus the possibilities of development of tachyarrhythmia. AMD therefore has its therapeutic and adverse effects both from prolongation of QT interval by inhibition of hERG currents, but the chances of adverse effect are markedly lowered because of enhancement of hERG currents during the afterdepolarization. It is of note that temperature has a critical action on the foregoing effect of AMD and also the molecular behaviors of the hERG channel themselves. In principle, lower temperatures or relevant pathophysiological/pharmacotherapeutic scenarios that slow or decrease hERG channel activation may readily jeopardize the unique afterdepolarization-preventing effect of AMD or even the essential physiologic function of hERG channels itself, and thus must be carefully handled with the foregoing rationales taken into consideration if encountered.

Authorship Contributions

Participated in research design: Lo, Kuo.
Conducted experiments: Lo.
Performed data analysis: Lo, Kuo.
Wrote or contributed to the writing of the manuscript: Lo, Kuo.

References

Babcock JJ and Li M (2013) hERG channel function: beyond long QT. *Acta Pharmacol Sin* **34**:329–335.

Bett GC, Zhou Q, and Rasmusson RL (2011) Models of HERG gating. *Biophys J* **101**:631–642.

Catterall WA (2010) Ion channel voltage sensors: structure, function, and pathophysiology. *Neuron* **67**:915–928.

Clancy CE and Rudy Y (2001) Cellular consequences of HERG mutations in the long QT syndrome: precursors to sudden cardiac death. *Cardiovasc Res* **50**:301–313.

Cuello LG, Jogini V, Cortes DM, and Perozo E (2010) Structural mechanism of C-type inactivation in K(+) channels. *Nature* **466**:203–208.

Furutani K, Yamakawa Y, Inanobe A, Iwata M, Ohno Y, and Kurachi Y (2011) A mechanism underlying compound-induced voltage shift in the current activation of hERG by antiarrhythmic agents. *Biochem Biophys Res Commun* **415**:141–146.

Heger JJ, Prystowsky EN, Jackman WM, Naccarelli GV, Warfel KA, Rinkenberger RL, and Zipes DP (1981) Clinical efficacy and electrophysiology during long-term therapy for recurrent ventricular tachycardia or ventricular fibrillation. *N Engl J Med* **305**:539–545.

Jiang M, Dun W, Fan JS, and Tseng GN (1999) Use-dependent "agonist" effect of azimilide on the HERG channel. *J Pharmacol Exp Ther* **291**:1324–1336.

Jiang M, Zhang M, Maslennikov IV, Liu J, Wu DM, Korolkova YV, Arseniev AS, Grishin EV, and Tseng GN (2005) Dynamic conformational changes of extracellular S5-P linkers in the hERG channel. *J Physiol* **569**:75–89.

Johnson JP Jr, Mullins FM, and Bennett PB (1999) Human ether-à-go-go-related gene K^+ channel gating probed with extracellular ca^{2+}: evidence for two distinct voltage sensors. *J Gen Physiol* **113**:565–580.

Kauthale RR, Dadarkar SS, Husain R, Karande VV, and Gatne MM (2015) Assessment of temperature-induced hERG channel blockade variation by drugs. *J Appl Toxicol* **35**:799–805.

Kiehn J, Thomas D, Karle CA, Schöls W, and Kübler W (1999) Inhibitory effects of the class III antiarrhythmic drug amiodarone on cloned HERG potassium channels. *Naunyn Schmiedebergs Arch Pharmacol* **359**:212–219.

Kuo CC, Chen WY, and Yang YC (2004) Block of tetrodotoxin-resistant Na^+ channel pore by multivalent cations: gating modification and Na^+ flow dependence. *J Gen Physiol* **124**:27–42.

Liu Y, Jurman ME, and Yellen G (1996) Dynamic rearrangement of the outer mouth of a K^+ channel during gating. *Neuron* **16**:859–867.

Lu Y, Mahaut-Smith MP, Varghese A, Huang CL, Kemp PR, and Vandenberg JI (2001) Effects of premature stimulation on HERG $K^{(+)}$ channels. *J Physiol* **537**:843–851.

Luo CH and Rudy Y (1994) A dynamic model of the cardiac ventricular action potential. I. Simulations of ionic currents and concentration changes. *Circ Res* **74**: 1071–1096.

McPate MJ, Duncan RS, Hancox JC, and Witchel HJ (2008) Pharmacology of the short QT syndrome N588K-hERG K^+ channel mutation: differential impact on selected class I and class III antiarrhythmic drugs. *Br J Pharmacol* **155**:957–966.

Milnes JT, Crociani O, Arcangeli A, Hancox JC, and Witchel HJ (2003) Blockade of HERG potassium currents by fluvoxamine: incomplete attenuation by S6 mutations at F656 or Y652. *Br J Pharmacol* **139**:887–898.

Mitcheson JS (2003) Drug binding to HERG channels: evidence for a "non-aromatic" binding site for fluvoxamine. *Br J Pharmacol* **139**:883–884.

Mitcheson JS, Chen J, Lin M, Culberson C, and Sanguinetti MC (2000) A structural basis for drug-induced long QT syndrome. *Proc Natl Acad Sci USA* **97**:12329–12333.

Perry MD, Ng CA, and Vandenberg JI (2013) Pore helices play a dynamic role as integrators of domain motion during Kv11.1 channel inactivation gating. *J Biol Chem* **288**:11482–11491.

Ridley JM, Milnes JT, Witchel HJ, and Hancox JC (2004) High affinity HERG $K^{(+)}$ channel blockade by the antiarrhythmic agent dronedarone: resistance to mutations of the S6 residues Y652 and F656. *Biochem Biophys Res Commun* **325**: 883–891.

Roden DM (2004) Drug-induced prolongation of the QT interval. *N Engl J Med* **350**: 1013–1022.

Sager PT, Uppal P, Follmer C, Antimisiaris M, Pruitt C, and Singh BN (1993) Frequency-dependent electrophysiologic effects of amiodarone in humans. *Circulation* **88**:1063–1071.

Sanguinetti MC, Jiang C, Curran ME, and Keating MT (1995) A mechanistic link between an inherited and an acquired cardiac arrhythmia: HERG encodes the IKr potassium channel. *Cell* **81**:299–307.

Schönherr R and Heinemann SH (1996) Molecular determinants for activation and inactivation of HERG, a human inward rectifier potassium channel. *J Physiol* **493**: 635–642.

Smith PL, Baukrowitz T, and Yellen G (1996) The inward rectification mechanism of the HERG cardiac potassium channel. *Nature* **379**:833–836.

Torres AM, Bansal PS, Sunde M, Clarke CE, Bursill JA, Smith DJ, Bauskin A, Breit SN, Campbell TJ, Alewood PF, et al. (2003) Structure of the HERG K^+ channel S5P extracellular linker: role of an amphipathic alpha-helix in C-type inactivation. *J Biol Chem* **278**:42136–42148.

Trudeau MC, Warmke JW, Ganetzky B, and Robertson GA (1995) HERG, a human inward rectifier in the voltage-gated potassium channel family. *Science* **269**:92–95.

Vandenberg JI, Torres AM, Campbell TJ, and Kuchel PW (2004) The HERG K^+ channel: progress in understanding the molecular basis of its unusual gating kinetics. *Eur Biophys J* **33**:89–97.

Wang S, Liu S, Morales MJ, Strauss HC, and Rasmusson RL (1997) A quantitative analysis of the activation and inactivation kinetics of HERG expressed in *Xenopus* oocytes. *J Physiol* **502**:45–60.

Yang YC, Hsieh JY, and Kuo CC (2009) The external pore loop interacts with S6 and S3-S4 linker in domain 4 to assume an essential role in gating control and anticonvulsant action in the $Na^{(+)}$ channel. *J Gen Physiol* **134**:95–113.

Yang YC and Kuo CC (2002) Inhibition of $Na^{(+)}$ current by imipramine and related compounds: different binding kinetics as an inactivation stabilizer and as an open channel blocker. *Mol Pharmacol* **62**:1228–1237.

Yang YC and Kuo CC (2005) An inactivation stabilizer of the Na+ channel acts as an opportunistic pore blocker modulated by external Na^+. *J Gen Physiol* **125**:465–481.

Zhang M, Liu J, and Tseng GN (2004) Gating charges in the activation and inactivation processes of the HERG channel. *J Gen Physiol* **124**:703–718.

Zhang Y, Colenso CK, El Harchi A, Cheng H, Witchel HJ, Dempsey CE, and Hancox JC (2016) Interactions between amiodarone and the hERG potassium channel pore determined with mutagenesis and in silico docking. *Biochem Pharmacol* **113**: 24–35.

Zimetbaum P (2007) Amiodarone for atrial fibrillation. *N Engl J Med* **356**:935–941.

Address correspondence to: Dr. Chung-Chin Kuo, National Taiwan University College of Medicine, No. 1 Jen-Ai Road, 1st Section, Taipei 100, Taiwan. E-mail: chungchinkuo@ntu.edu.tw

Supplemental Data

Title: Temperature dependence of the biophysical mechanisms underlying the inhibition and enhancement effect of amiodarone on hERG channels

Authors: Yung-Chen Lo and Chung-Chin Kuo

Journal title: Molecular Pharmacology

SUPPLEMENTAL FIGURE LEGENDS:

Supplemental figure 1. (A) Sample sweep of hERG currents in control (black), 0.2% DMSO, and 2% DMSO (red) are shown. The holding potential is -120 mV and the test pulse is 0 mV × 30-sec. (B) and (C) The current amplitude at 100 ms (part B) and 30 sec (part C) of the test pulse in different concentrations of DMSO is normalized to that in control to give the relative current. Note the (~10%) enhancement effect of 2% DMSO at 100 ms. and the (~5%) inhibitory effect of 2% DMSO at 30 sec. The effect of 0.2 % DMSO is negligible (all n=4).

Supplemental figure 2. Dose-dependent inhibition of AMD on hERG currents with a mild and prolonged depolarization pulse. (A) hERG currents were elicited by a prolonged test pulse (120 sec) to -60, -50, -40, -30 mV from a holding potential of -90 mV in control and in different concentrations (1-100 μM) of AMD. (B) The sustained and (peak) tail currents at -90 mV in different concentrations of AMD are normalized to that in control to give the relative current (n=4). (C) With a -30 mV test pulse, lengthening of test pulse to 120 sec could not slow the deactivation tau further (305±21 ms in control and 259±9 ms in 10 μM AMD, if compared to that in Fig. 1 B) (n=4). In contrast, the deactivation tau at -60 mV is markedly slowed by prolongation of the -60 mVtest pulse to 120 sec (269±12 ms in control and 292±37 ms in 10 μM AMD), if compared to that in Fig. 1 C (n=4).

Supplemental figure 3. The G-V relationships of hERG current at 22 °C and 37 °C with and without 10 μM AMD. (A) and (B) are sample hERG currents elicited with a pulse protocol comprised of 0.3-sec and 3.3-sec test pulses from -60 to +60 mV (in 10 mV step) from a holding potential at -90 mV at 37 °C (part A) and 22 °C (part B). (C) and (D) The late sustained, (the average currents in the last 5 ms, (part C) and the peak tail currents at -90 mV (part D) in control and AMD are normalized to that at the +60 mV test pulse (part C) or following the +60 mV test pulse in control in the same cell to obtain the relative current which is then plotted against the test pulse voltage to give the G-V curve (all n=4).

Supplemental figure 4. Concentrations -dependent enhancement effect of AMD on the initial activation rate of hERG channels with a (200 ms) test pulse at 0 mV. (A) The hERG currents at the 200 ms test pulse from a holding potential of -120 mV is concentration-dependently enhanced by AMD at 22 °C. The intersweep interval is 1.5-3.5 min, which is enough to fully recover all inactivated channels back to the resting state. (B) The peak current amplitude at the test (upper panel) and tail pulse (lower panel) in different concentrations of AMD is normalized to that in control to give the relative current, which is then plotted against AMD concentration (n=4, *paired t-test, $p<0.05$)

Supplemental figure 5. (A) hERG currents were elicited by a test pulse to +30 or +60 mV from a holding potential of -90 mV at 22 °C. At both test pulse voltages the test pulses are lengthened from 1 to 5 secs (Δt=1 sec) and then to 10 seconds before returning to -90 mV to measure the tail currents. Note the acceleration of current decay at +30 mV prepulse by 10 μM AMD. AMD, however, has no apparent effect on the currents at +60 mV prepulse, where the currents in control already show a prominent initial decay. On the other hand, the inward tail currents are gradually inhibited by 10 μM AMD with lengthening of the test pulse, no matter it is +30 or +60 mV. (B) The decay phase of the macroscopic currents in the +30 mV test pulse in 10 μM AMD is fitted by the mono-exponential function (tau = 2.0 secs). The peak tail currents in 10 μM AMD following either a +30 or +60 test pulse are normalized to the first one to obtain the relative current, which is then plotted against test pulse duration and fitted with a mono-exponential function with a time constant of 2.8 and 2.3 secs, respectively (each n=4).

Supplemental figure 6. (A) with a pulse protocol similar to that in Fig. 4A, the prepulse was set at 0 mV × 8 sec, and the gap duration was lengthened from 3 to 192 secs. The enhancement effect of 10 μM AMD on hERG current during the test pulse at -60 mV is decreased with lengthening of the gap duration. (B) and (C)The currents in the test pulse (part B) and the following tail currents (part C) are normalized to the maximal one (that with a gap duration of 3 secs) to give the relative currents, which are

plotted against gap duration and fitted with mono-exponential functions (n=4). Note that the time constant is much larger (the decrease of the enhancement effect is much slower) in the presence of 10 μM AMD than in control.

Supplemental figure 1

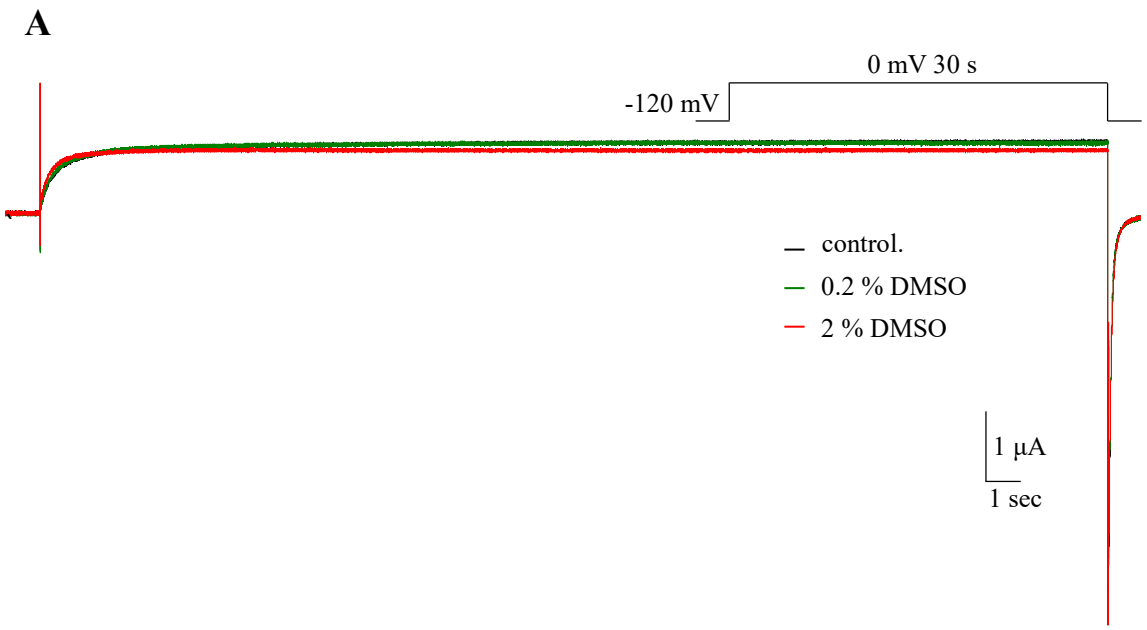

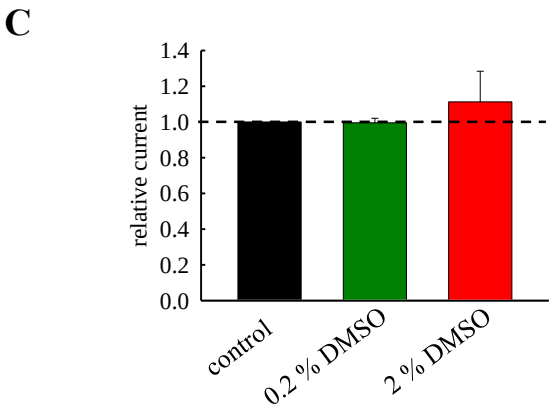

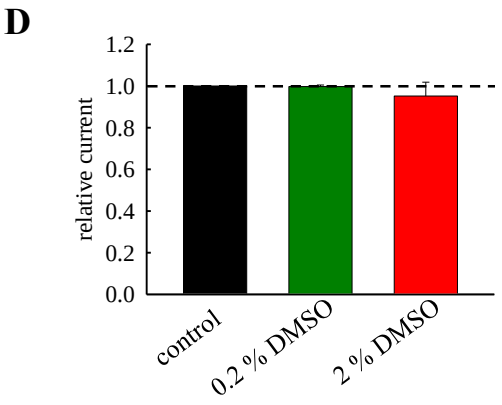

Supplemental figure 2

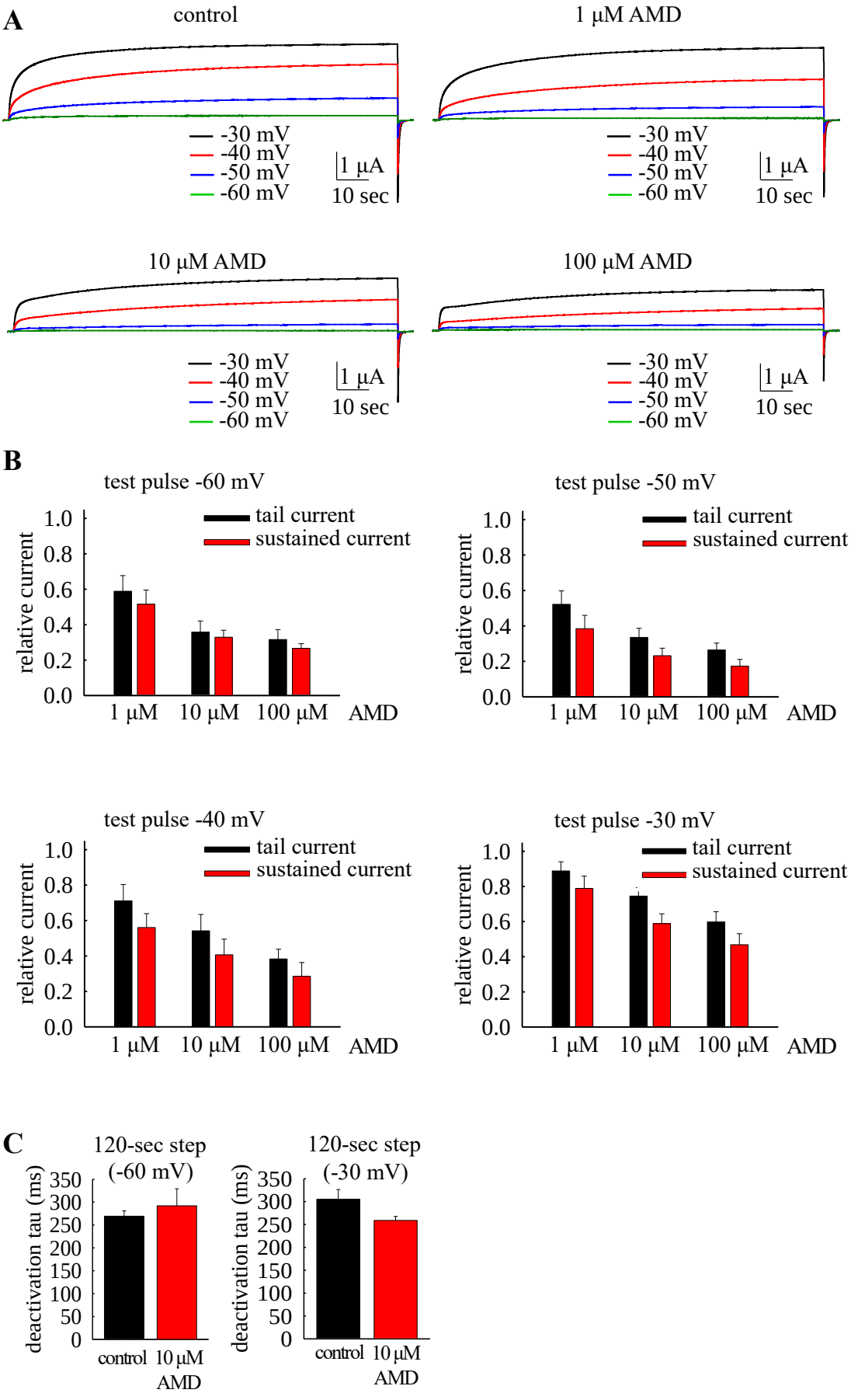

Supplemental figure 3

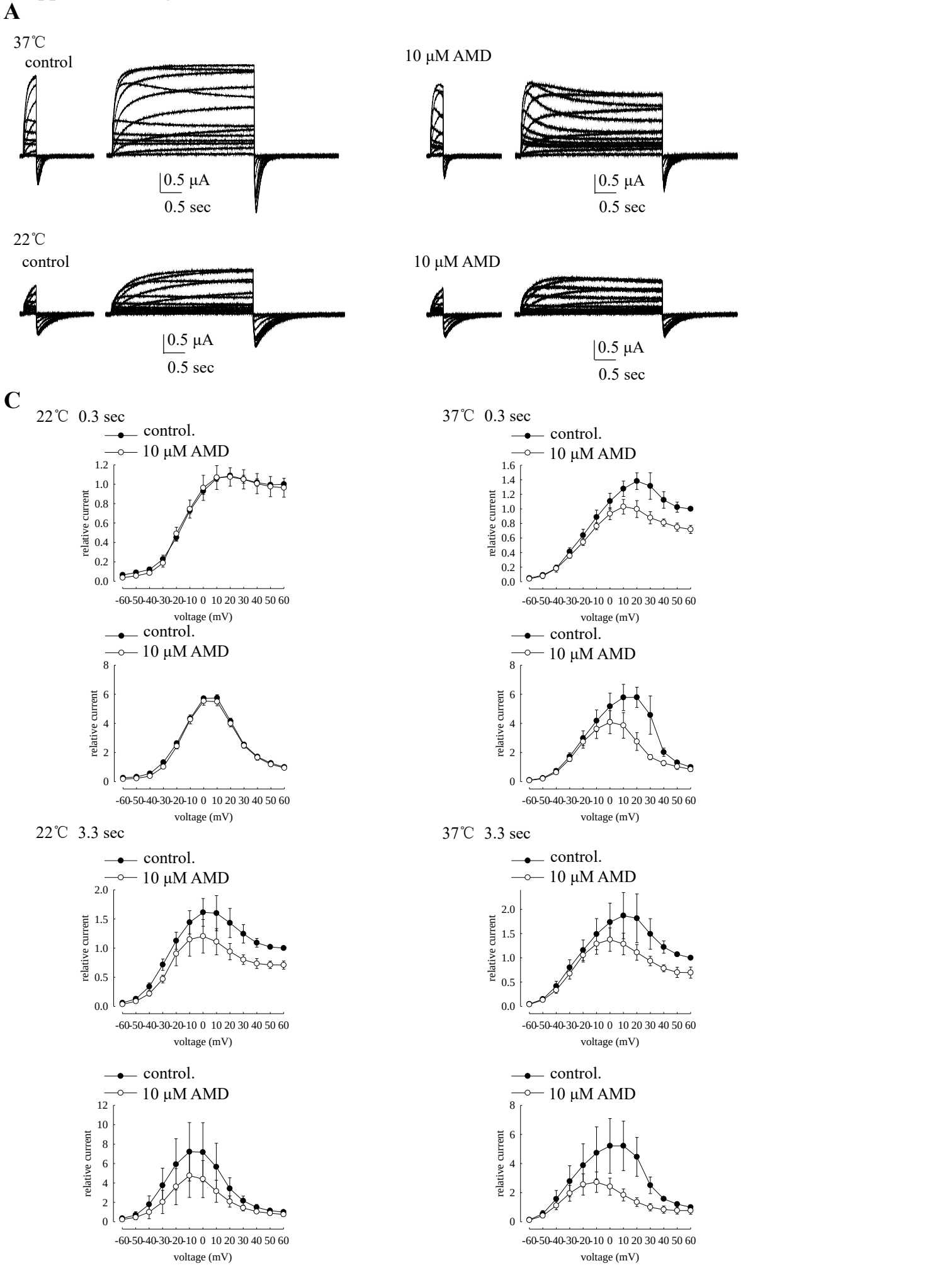

Supplemental figure 4

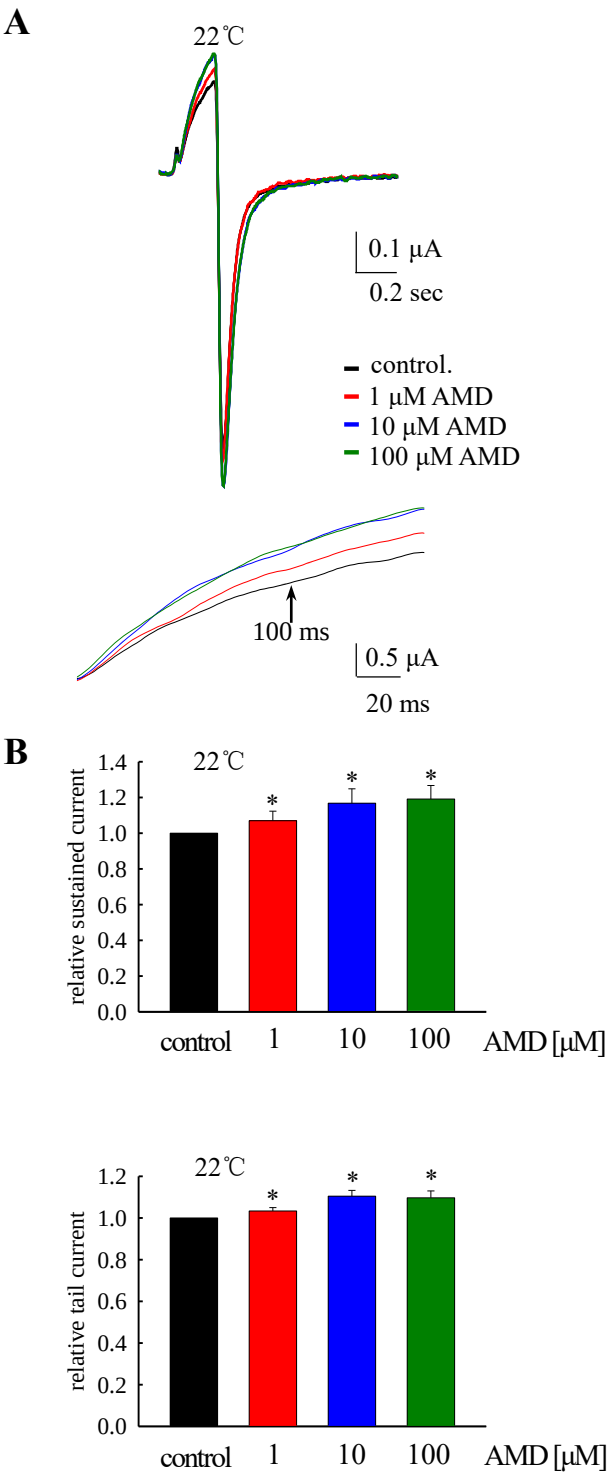

Supplemental figure 5

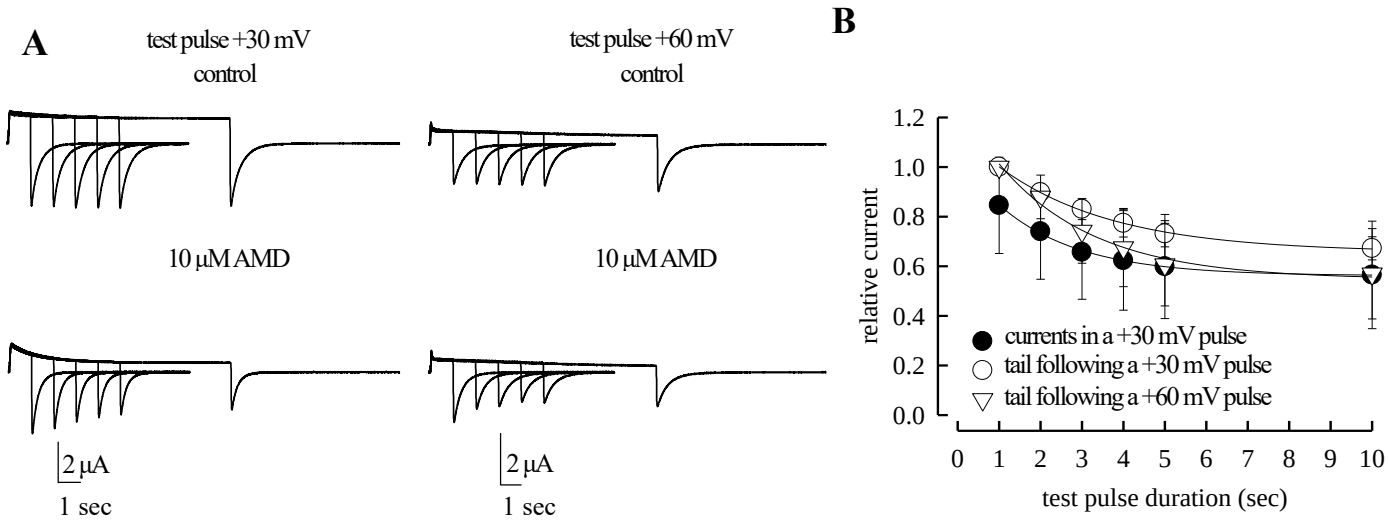

Supplemental figure 6